DESIGN AND ANALYSIS OF A FULL SCALE AIR VITIATOR FOR HIGH SPEED WIND TUNNEL

A THESIS SUBMITTED TO
THE GRADUATE SCHOOL OF NATURAL AND APPLIED SCIENCES
OF
MIDDLE EAST TECHNICAL UNIVERSITY

BY

MURAT BAYRAMOĞLU

IN PARTIAL FULFILLMENT OF THE REQUIREMENTS
FOR
THE DEGREE OF MASTER OF SCIENCE
IN
AEROSPACE ENGINEERING

JUNE 2011

Approval of the thesis:

DESIGN AND ANALYSIS OF A FULL SCALE AIR VITIATOR FOR HIGH SPEED WIND TUNNEL

submitted by **MURAT BAYRAMOĞLU**, in partial fulfillment of the requirements for the degree of **Master of Science in Aerospace Engineering Department, Middle East Technical University** by,

Prof. Dr. Canan ÖZGEN _____
Dean, Graduate School of **Natural and Applied Sciences**

Prof. Dr. Ozan TEKİNALP _____
Head of Department, **Aerospace Engineering**

Prof. Dr. Sinan AKMANDOR _____
Supervisor, **Aerospace Engineering Dept., METU**

Assist. Prof. Dr. Oğuz UZOL _____
Co-supervisor, **Aerospace Engineering Dept., METU**

Examining Committee Members:

Prof. Dr. Cevdet ÇELENLİGİL _____
Aerospace Engineering Dept., METU

Prof. Dr. Sinan AKMANDOR _____
Supervisor, Aerospace Engineering Dept., METU

Assist. Prof. Dr. Sıtkı USLU _____
Mechanical Engineering Dept., TOBB EDU

Assoc. Prof. Dr. Abdullah ULAS _____
Mechanical Engineering Dept., METU

Assist. Prof. Dr. Oğuz UZOL _____
Co-supervisor, Aerospace Engineering Dept., METU

Date: 23.06.2011

I hereby declare that all information in this document has been obtained and presented in accordance with academic rules and ethical conduct. I also declare that, as required by these rules and conduct, I have fully cited and referenced all material and results that are not original to this work.

Name, Last Name: MURAT BAYRAMOĞLU

Signature :

ABSTRACT

DESIGN AND ANALYSIS OF A FULL SCALE AIR VITIATOR
FOR HIGH SPEED WIND TUNNEL

Bayramoğlu, Murat
M. Sc., Department of Aerospace Engineering
Supervisor : Prof. Dr. Sinan Akmandor
Co-Supervisor : Assist. Prof. Dr. Oğuz Uzol

June 2011, 89 pages

The aim of this thesis is to develop a combustion type air heater, namely vitiator, for high speed wind tunnel. The high speed wind tunnel test setup is capable of feeding more than 2 minutes high pressure and high temperature air. High temperature air is conditioned with the vitiator.

Initially an analytical design methodology was constituted for the vitiator. After the design, CFD simulations of the reactive flows were performed. The vitiator was manufactured and tested after the CFD analysis. Tests were performed with a prototype vitiator feeding system.

Control system and data acquisition software were also developed for this feeding system. Thermocouple data was collected at the end of the vitiator. A camera system was used to monitor the vitiator during the tests. It is observed that vitiator can work successfully for a wide range of operating conditions. It is also verified that prototype feeding system can work efficiently. Any flame can be observed at the end of the vitiator. This indicates that combustion is completed in the vitiator and combustion efficiency high enough.

Key-words: High speed wind tunnel, reactive flow CFD analysis, vitiator

ÖZ

YÜKSEK HIZLI RÜZGAR TÜNELİ İÇİN
HAVA ISITICISI TASARIMI VE ANALİZİ

Bayramoğlu, Murat
Yüksek Lisans, Havacılık ve Uzay Mühendisliği Bölümü
Tez Yöneticisi: Prof. Dr. Sinan Akmandor
Ortak Tez Yöneticisi: Yrd. Doç. Dr. Oğuz Uzol

Haziran 2011, 89 sayfa

Bu tez kapsamında, yüksek hızlı rüzgar tünellerinda kullanılmak için gerekli hava ısıtıcısı geliştirilmiştir. Yüksek hızlı rüzgar tüneli ile, 2 dakikanın üzerinde yüksek basınçta ve yüksek sıcaklıkta hava sağlanmaktadır. Havanın sıcaklığı hava ısıtıcısı ile arttırılmaktadır.

İlk olarak hava ısıtıcısı için analitik tasarım yöntemi geliştirilmiştir. Tasarım tamamlandıktan sonra reaktif Hesaplamalı Akışkanlar Dinamiği (HAD) analizleri gerçekleştirilmiştir. HAD analizlerinin tamamlanmasının ardından hava ısıtıcısı üretilmiş ve daha sonra test faaliyetlerine başlanmıştır.

Testler için prototip besleme sistemi geliştirilmştir. Besleme sisteminin kontrolü için Labview yazılımı ve modüler veri toplama sistemi kullanılmıştır. Testler

sırasında ısıtıcının sonundan ısıl çiftler ile yanma odası ortalama çıkış sıcaklıkları ölçülmüştür. Isıtıcının başarıyla çalıştığı gösterilmiştir. Isıtıcıyı çalıştıran prototip besleme sisteminin verimli şekilde çalıştığı görülmüştür. Isıtıcı dışarısında alev gözlenmemiştir. Bu durum ısıtıcının yanma veriminin yüksek olduğu şeklinde değerlendirilmiştir.

Anahtar Kelimeler: Yüksek hızlı rüzgar tüneli, reaktif Hesaplamalı Akışkanlar Dinamiği analizleri, hava ısıtıcısı

Aileme ve eşim Kübra’ya,

ACKNOWLEDGEMENT

I would like to express my gratitude and strong patient to Prof. Dr. Sinan AKMANDOR for his supervision through this thesis.

I would like to thank to my co-supervisor Assoc. Prof. Dr. Oğuz UZOL, for his advises.

I would like to express my sincere appreciation to Assoc. Prof. Dr. Sıtkı USLU for worthy and precious helps on CFD modeling of the problem.

I would also like to thank to my brothers Başar ESİRGEN, Utku OLGUN and Metin ARSLAN for endless helps of coding CCDC, reacting CFD analyses, design and tests. This was impossible without you…

I would also like to express my gratitude to big boss Dr. Kemal Atılgan TOKER who motivated us and gave opportunities to accomplish our dreams.

Special thanks to my family who always encouraged me to get highest education in the life.

And very special thanks go to my beautiful wife Kübra who motivated me for nights to complete this thesis when I came home tired and lazy.

This thesis is dedicated to my family and wife, I ever never remunerate of you.

TABLE OF CONTENTS

LIST OF TABLES

TABLES

LIST OF FIGURES

FIGURES

LIST OF SYMBOLS

$\dot{Q}_{CV}$	Heat transfer rate across the control surface from the surroundings, to the control volume
$\dot{W}_{CV}$	Work rate done by the control volume, including shaft work, but excluding flow work
$\dot{m}e_o$	Energy rate coming out of the control volume
$\dot{m}e_i$	Rate of energy coming into the control volume
MM_{air}	Molecular mass of the air
MM_{fuel}	Molecular mass of the fuel
$(A/F)_{stoic}$	Stoichiometric Air to Fuel ratio
ϕ	Equivalence Ratio
A/F	Air to Fuel Ratio
T_{ref}	Standard reference temperature
P_{ref}	Standard reference pressure
h_f	Enthalpy of formation
Δh_s	The sensible enthalpy change
Δh_R	Enthalpy of combustion
Δh_C	Heat of combustion
ν'_j	The stoichiometric coefficient of the reactants
ν''_j	The stoichiometric coefficients of the products
RR	Reaction Rate
Z_{AB}	Gas kinetic collision frequency
$\exp(-E/RT)$	Boltzmann factor
E_A	Activation energy

σ_{AB}	Hard sphere collision diameter
k	Boltzmann constant
μ	Reduced mass
$\wp$	Steric factor
n	Pressure exponent, mole number, number of swirler vanes
U	Velocity through the Cooling Air Holes
d	Diameter of the Cooling Air Holes
d_h	Hydraulic diameter of the cooling air holes
C_d	Discharger Coefficient
K_{sw}	Flat Plate Vane Coefficient
θ	Vane Angle
A_L	Combustion Chamber Liner Wet Area
A_{sw}	Inlet Area of the swirler
D_{sw}	Outer diameter of the swirler
D_{hub}	Inner diameter of the swirler
t	Swirler vane thickness, wall thickness of liner
γ	Specific Heat Ratio
σ	Stefan Boltzmann constant
e_w	Emissivity of the Liner
e_g	Emissivity of the Combustion Products
e_c	Emissivity of the Casing
T_g	Temperature of the products
T_{w1}	Inner wall temperature
T_{w2}	Outer wall temperature
T_3	Ambient air temperature

μ_{ug}	Viscosity of cooling air
k_a	Conductivity of cooling air
k_g	Conductivity of combustion air
k_w	Conductivity of the liner
A_{an}	Cross section area of cooling air flow passage
A_l	Cross section Area of Combustion Chamber
ΔPcc	Maximum Pressure Drop of the combustion chamber
$\Delta Psch$	Pressure loss sourced by cooling holes
L/D	Length to Diameter Ratio
C_{in}	Convective Heat Flux from Hot gases to Liner
C_{ex}	Convective Heat Flux from liner to Cooling Jacket
R_{in}	Radiative Heat Flux from hot gases to liner
R_{ex}	Radiative Heat Flux from Liner to Cooling Jacket
K_{1-2}	Conductive Heat Flux through the liner

Subscripts

in	Inlet
ex	Exit
i	Reactants
o	Products
g	Gas
c	Casing
sw	Swirler
hub	Hub of the swirler

Abbreviations

SSSF	Steady State Steady Flow
CCDC	Combustion Chamber Design Code
CLP	Combustion Loading Parameter
CC	Combustion Chamber
SN	Swirl Number
CAH	Cooling Air Holes
FIP	Fuel Injector Position
CCDA	Combustion Chamber Divergence Angle
SVA	Swirl Vane Angle

CHAPTER 1

INTRODUCTION

1.1 Purpose of the Thesis

The purpose of this thesis is to develop an air heater, namely vitiator, which is used for high speed wind tunnels. For this kind of tunnels it is necessary to use a high capacity air supply and to simulate high speed conditions behind the shock waves, air heaters. Different kinds of air heaters are being used in the world for different purposes.

- Combustion type air heaters
- Capacitive type air heaters
- Electrical air heaters

For simplicity and efficiency, combustion types of air heaters are mostly preferable in the high speed propulsion system test setups in the world. In this thesis a general literature survey is performed for determining the best choice of air heater. An analytical design methodology is constructed and a Combustion Chamber Design Code is developed. Reactive Flow CFD analyses are performed after the designing the combustion chamber. With completion of the design and analysis, tests are performed to check if the vitiator works properly.

1.2 Content of the Thesis

In Chapter 2, a literature survey for the vitiator is given. Characteristics of the vitiator are explained. Advantages and disadvantages of the vitiator are clarified and different famous test setups and heaters are introduced in this chapter.

Combustion background is introduced in Chapter 3 and thermochemistry of combustion is explained. Scientific disciplines comprising combustion are briefly described. Mass transfer and chemical kinetics are introduced briefly and methane combustion is investigated.

Thermodynamic model of the vitiator is constructed in Chapter 4. Combustion Chamber Design Code (CCDC), the modules of CCDC and the design drivers are introduced. The results are presented and important points are emphasized. Finally the design of the heater is explained in this chapter.

Reacting flow CFD analyses are introduced in Chapter 5. Analysis methodology and results are clearly explained.

Initial test results of the vitiator are given in Chapter 6. Important observations are pointed to at the end of this chapter.

Conclusion and discussion section is given in Chapter 7. Also the possible future works are offered in this chapter.

CHAPTER 2

LITERATURE SURVEY

2.1 Brief Description of High Speed Wind Tunnels

Air heaters are used to high speed wind tunnels for conditioning the air in terms of pressure and temperature. On wind tunnels there must be a control and data acquisition system to perform the tests correctly. High speed wind tunnels basically include the following subsystems:

- Air Supply System
- Air Heater
- Control System
- Data Acquisition System

Even though the air supply, control and data acquisition systems are almost similar, air heaters shows differences for various wind tunnels. Air heaters may be combined under three main headlines as follows:

- Combustion Heaters (Vitiators),
- Pebble Bed Heaters
- Electric Heaters (Arc Heaters)

Only the vitiator is considered in this thesis.

2.2 Characteristics of the Vitiator

For the appropriate simulation of vehicle flight conditions, the air must be supplied at the stagnation temperatures and pressures that are to be encountered during flight. An air heater is used to increase the air temperature to simulate the conditions produced by a supersonic compression, where the heater supplies the required high temperature and high pressure air. Vitiators are the combustion chambers which heats the air simply by a combustion reaction. A schematic representation is given in Figure 2.1.

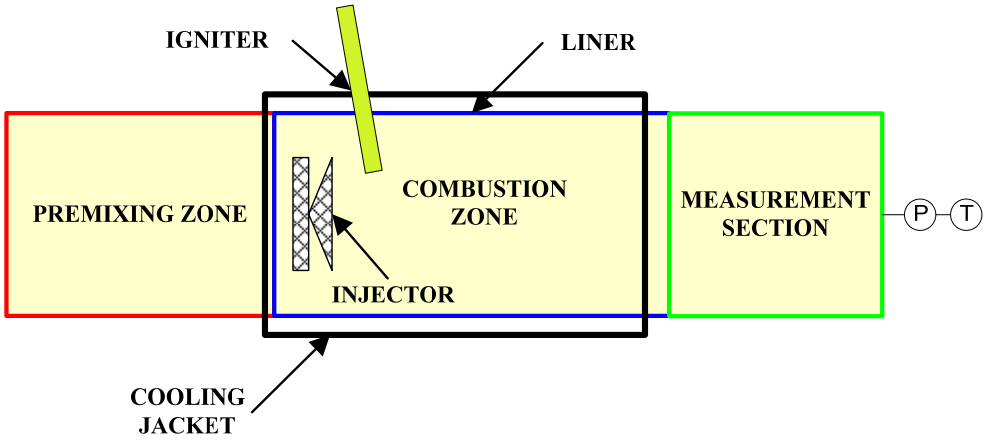

Figure 2.1 Schematic Representation of the Vitiator

Operation of the vitiator can be summarized as follows:

- Fuel supplied to the injector.
- Replenishment oxygen is given to the vitiator.
- Fuel air mixture is ignited via an igniter in the combustion chamber.
- Air is heated to the result of the combustion reaction.
- Heated air is send to the test unit after measuring the temperature and pressure.

To keep the oxygen molar ratio same of the cold and heated air, extra oxygen is given to the vitiator, namely replenishment oxygen.

The advantages of using Vitiator can be summarized as follows [6]:

- Easy to simulate different altitudes and Mach numbers
- Low fuel consumption
- Low cost
- Easy for operation
- Ease for maintenance

The disadvantages of using Vitiator are as follows [6]:

- Combustion products (basically H_2O vapor and CO_2) may differ the air characteristics
- The unburned fuel and some by-products (mainly CO) may affect the ramjet combustor performance

Some important high speed wind test setups are introduced and main applications are described in this section. A summary table is given at the end of this part.

2.3 WPAB Supersonic Combustion Research Facility

Recently developed United States Air Forces Wright Patterson Air Base Supersonic Combustion Research Facility shown in Figure 2.2. This facility is called as Test Cell 22 and is mainly used for scramjet development program. Test cell 22 is also used for development of ramjet or turbo-ramjet engines which diameter is smaller than 0.127m. Following studies were performed in this facility for the scramjet engines [1]:

- Supersonic fuel injection,
- Flame holding mechanisms
- Supersonic ignition
- Insulation between air intake-combustion chamber

- Shock-Boundary layer interaction
- Other hypersonic system component studies

Mach 7 and higher Mach numbers can be modeled in the facility by using 4 different nozzles. 13.6kg/s, 923K and 52Bar air can be supplied to the test unit. Air is heated with a vitiator which uses natural gas (mainly methane). Replenishment oxygen is given to the heated air. The total temperature and pressure of the air is measured by water cooled probes. Vitiator also can be worked with hydrogen and jet propellant [2]. Test Cell 22 and scramjet combustor test rig is shown in Figure 2.2 and Figure 2.3 respectively.

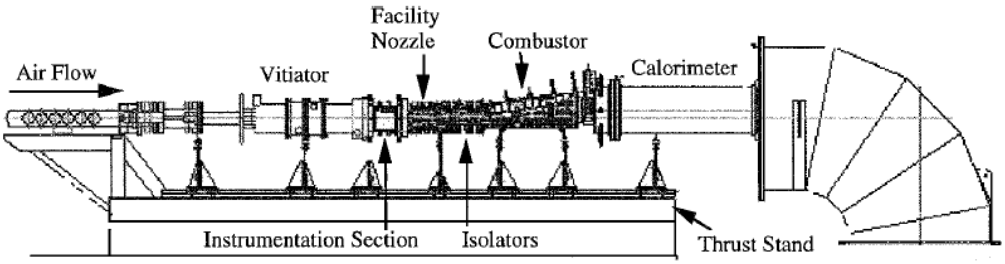

Figure 2.2 United States Air Force WPAB Supersonic Combustion Test Facility

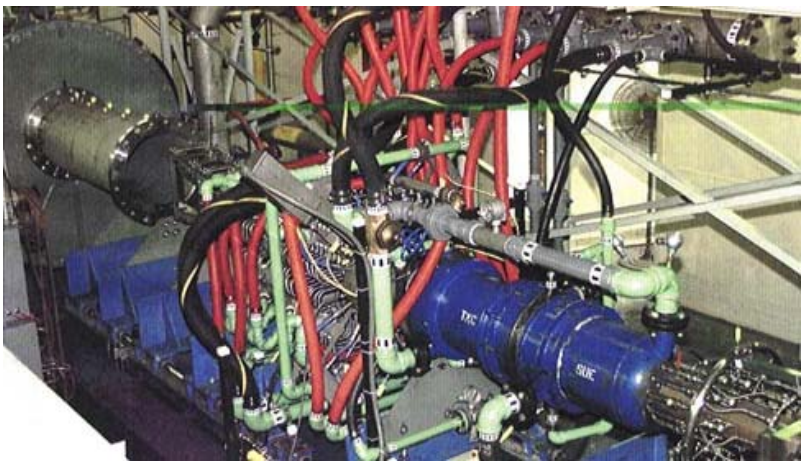

Figure 2.3 View of the Vitiator

The main subsystems of the Test Cell 22 can be given as follows [3]:

- Kaiser-Marquardt Sudden Expansion (SUE®)Vitiator
- Measurement Section
- Inlet transition flange and Supersonic Nozzle Section
- Isolator sections
- Calibration section
- Variable Configuration Combustion Chamber

SUE® Vitiator which was developed by Marquardt Company is shown in Figure 2.4. It is used a Hydrogen/Oxygen pilot flame igniter. SUE® vitiator has a water cooled combustion chamber and this chamber can resist 2500K temperature.

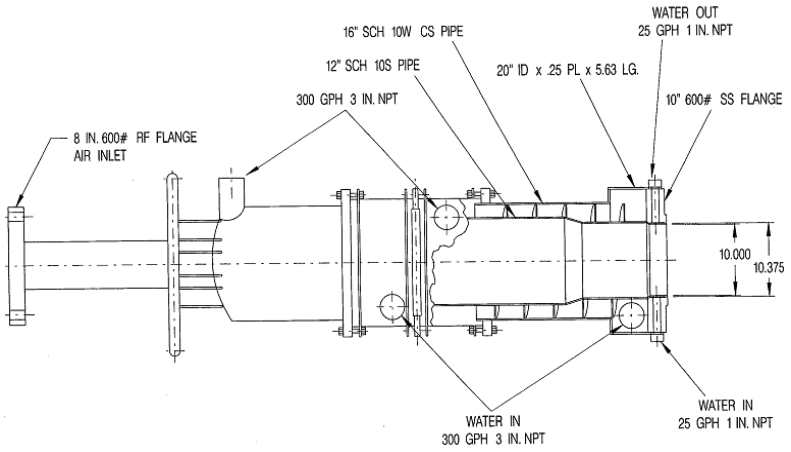

Figure 2.4 Kaiser Marquardt SUE® Vitiator Schematic Representation

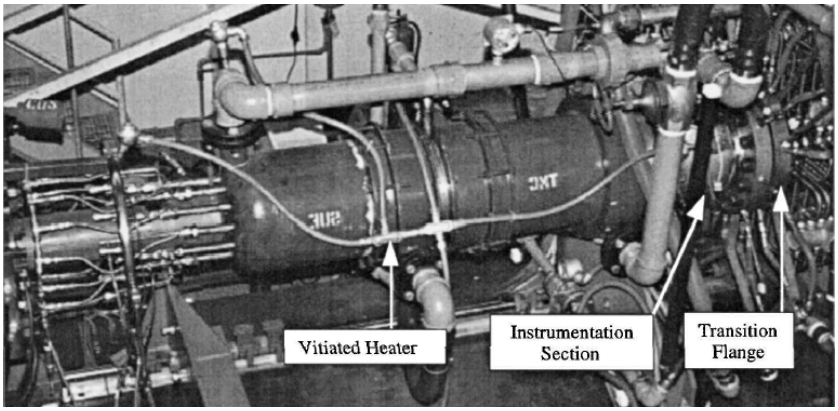

Figure 2.5 Kaiser Marquardt's SUE® Vitiator

2.4 NPS Rocket Propulsion and Combustion Laboratory

Naval Post Graduate School Rocket Propulsion and Combustion Laboratory comprises 2 cold test rooms, 3 combustion experiments rooms and a control& monitoring room. An optically accessible solid propellant ramjet engine test setup is given in Figure 2.6. Air storage capacity of this facility is 5.66 m3 and 3.63kg/s air can be given to the test unit. The cold air is heated by Hydrogen/Oxygen vitiator. The vitiator can increase the temperature of the air up to 811K. Ramjet, scramjet and pulse detonation engines flight simulations can be done with this kind of test setup [4]. Different kinds of diagnostic systems are included in this facility and these can be summarized as follows: [4]

- Phase Doppler Particle Analyzer (PDPA)
- Malvern Particle Analyzer
- High Speed Increased Sensitivity CCD cameras
- Infrared Monitoring Systems
- Spectroradiometers
- PIV and Wide Scale Laser Systems

Secret projects of American Ministry of Defense and Navy were performed in this laboratory. Lots of very first projects were carried out in this laboratory are summarized as follows:[4,5]

- First successful solid propellant scramjet engine ignition
- Smoke reducing additives research for the gas turbine engine propellants (this additive is used by the American Navy)
- First solid propellant gas generator supersonic combustion chamber ignition
- First pulse detonation engine ignition with JP-10 in room temperature
- Acceleration effect on double based propellant combustion
- Investigation of spatial distribution of the particles in the solid propellant rocket motor plume

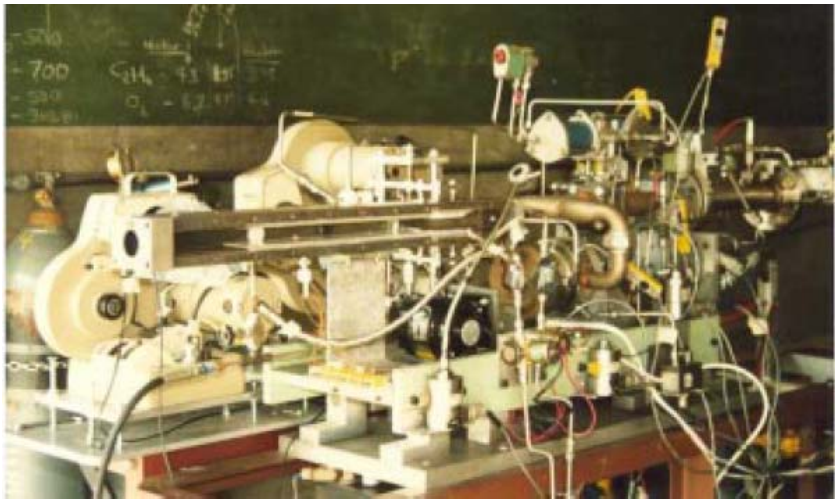

Figure 2.6 NPS Optically Accessible Ramjet Combustion Test Setup

2.5 NASA Langley's Direct-Connect Supersonic Combustion Test Facility

Ramjet and scramjet engines can be tested in NASA Langley Direct Connect Supersonic Combustion Test Facility (DCSCTF) in the 4-7.5mach conditions. This facility is schematically given in Figure 2.7.

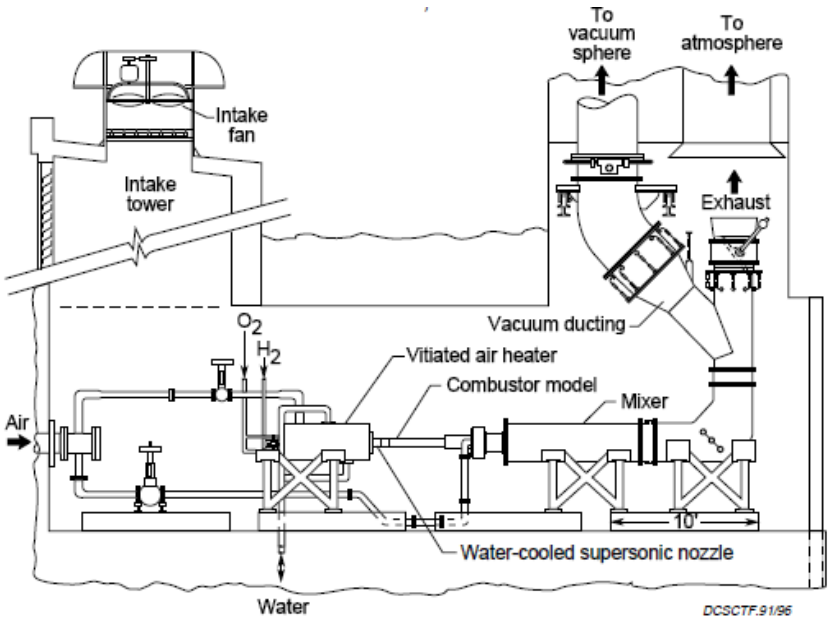

Figure 2.7 NASA Langley Direct Connect Supersonic Combustion Test Facility

Air is supplied to the test setup from a pressurized air tanks and nominal value of pressurized air is set to 38Bar. Air is heated up to 2000K by a Vitiator which uses Hydrogen as propellant and the feeding lines purged by Nitrogen. Also replenishment oxygen is given to the vitiator. H_2 and O_2 are supplied from the 162.5Bar industrial tanks and the pressure is reduced to initial value of 50Bar. Purging nitrogen is too supplied from 165.5Bar industrial tanks and is reduced to 16 Bar for purging. [7].

Main vitiator is shown in Figure 2.8 schematically. Replenishment oxygen is injected to the incoming air and a pre-mixture is provided. Hydrogen is injected to the air-oxygen pre-mixture. Vitiator is cooled by water. A pilot flame igniter is used to start combustion. H_2 and O_2 is used as propellant for the igniter. [7]

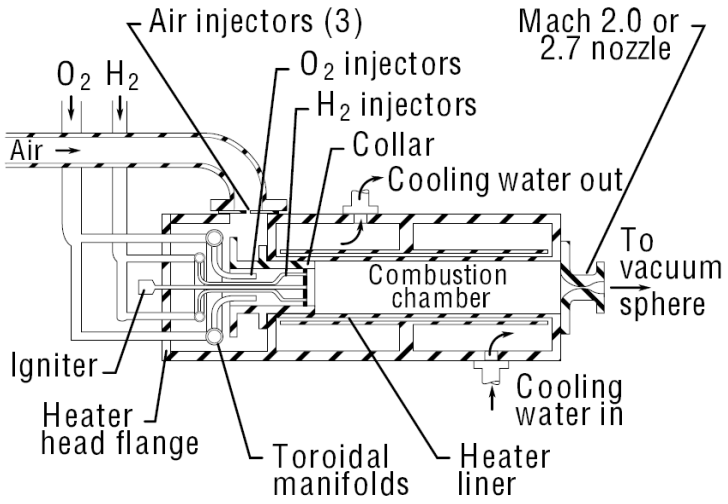

Figure 2.8 Schematical Representation DCSCTF Vitiator

Various nozzles can be added to the test setup to simulate scramjet conditions. Necessary vacuum for the altitude simulation is provided with an ejector facility which has a 31.34m diameter vacuum chamber. This system necessitates 11340kg/h water vapor. [7].

2.6 NASA Langley the 8-Foot High Temperature Tunnel

The 8 Foot High temperature Tunnel has been built in 1950's and operationally started to work in 1965's. The facility directed the aerothermal and aerothermomechanical studies for a long time. Methane is used for the propellant in this facility and Mach 7 conditions can be simulated. Oxygen replenishment system and 2 new nozzles were added to the facility in 1990's. System became capable of simulate Mach 4 and 5 conditions with this attachments. [8]

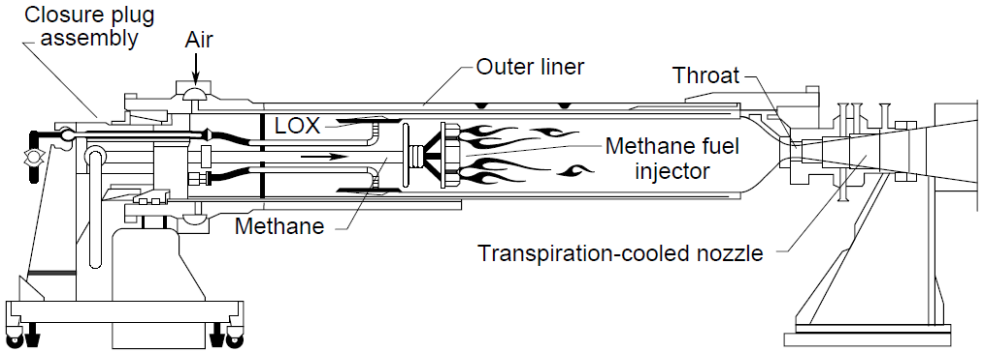

Figure 2.9 Shematic Representation of 8-Foot High Temperature Tunnel Vitiator

2.7 AEDC Aerodynamic and Propulsion Test Unit (AEDC-APTU)

Arnold Engineering Development Center; Aerodynamic and Propulsion Test Unit—AEDC; APTU), is a test unit which allows to the high temperature aerodynamic, propulsion and material tests. A hydrogen vitiator is used in this facility and replenishment oxygen is given to the vitiator. A free jet nozzle can be attached to the tail part of the vitiator. Schematic representation of vitiator and test setup configuration is given in Figure 2.10 [9]. AEDC-APTU is a completely computer controlled facility and temperature and pressure values are set in a very short time [9]. AEDC-APTU has air storage capacity of 6623m3 and 262Bar. Test runs can be between 3-12 minutes. Test differs according to flight Mach number and flight altitude. [9]

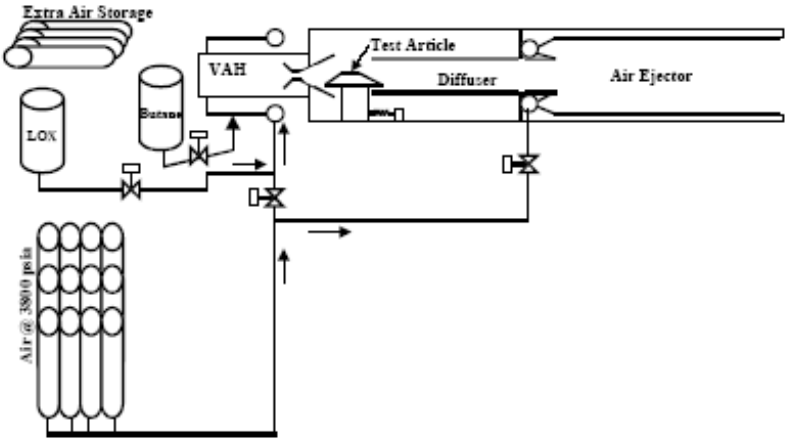

Figure 2.10 AEDC-APTU Free Jet Test Setup

2.8 United Technologies Research Center (UTRC) Scramjet Test Setup

The aim of the United Technologies Research Center (UTRC) Scramjet Test Setup is to constitute a rational approach to the supersonic combustor design and analyses. Advanced diagnostic techniques are used in the facility. These techniques allow measuring combustion parameters in detailed [10].

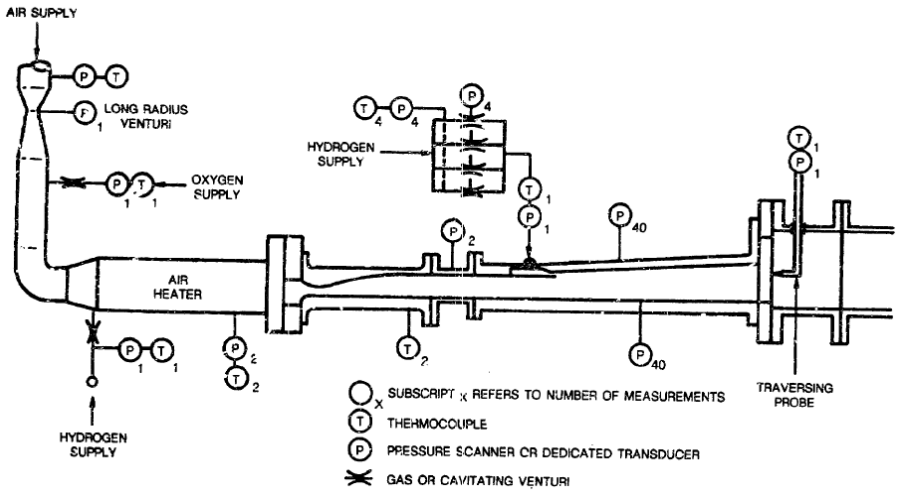

Figure 2.11 United Technologies Research Center Scramjet Test Setup

2.9 CAS Laboratory of High Temperature Gas Dynamics

"Chinese Academy of Sciences High Temperature Gas dynamics Test Setup" is mainly designed for the scramjet combustor tests. 8 different scramjet combustors have been designed for the tests. Tests are performed for different stagnation conditions and equivalence ratios. Stagnation temperature is set in the range of 1200-200K, stagnation pressure 10-14Bar and equivalence ratio from lean limits to rich limits [11]. Considering short residence times in the combustion chambers, complete combustion process is searched. High temperature air is obtained via hydrogen fueled vitiator. Replenishment oxygen is added to the vitiator. Vitiator can supply 2100K, 45Bar and 2kg/s conditioned air. Schematic representation of the vitiator and test setup is given in Figure 2.12 [11].

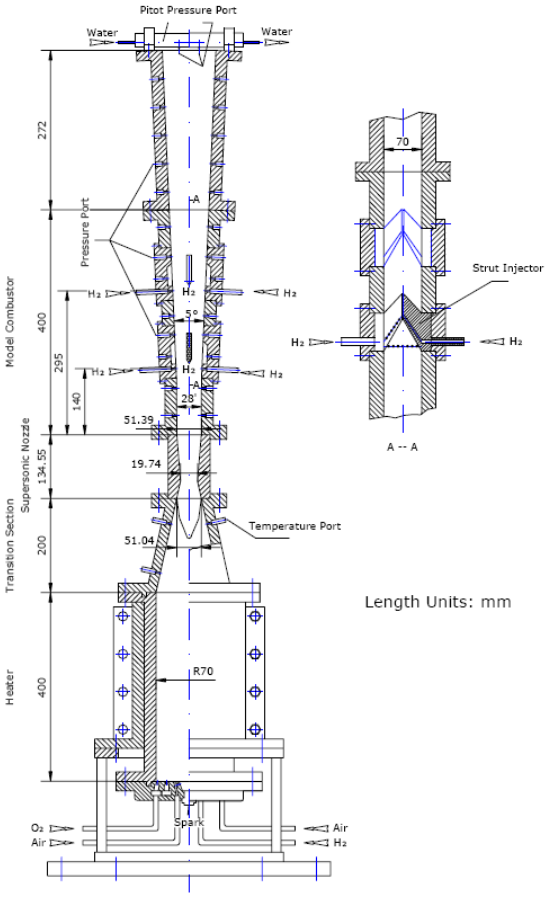

Figure 2.12 CAS Supersonic Combustor Test Setup

2.10 John Hopkins High Speed Aerothermal and Propulsion Test Laboratory

John Hopkins University High-Speed Aerothermal and Propulsion Test Laboratory supports air breathing propulsion system tests more than 35 years. Combustion chamber, fuel injector and nozzle are tested component by component or as a single system. More recently, this setup is used for the IR sensor tests. Schematic representation of the test setup is given in Figure 2.13.

In this facility Mach 4 – 5 conditions can be simulated. Hot air is obtained by the hydrogen fueled vitiator. Air can be heated up to 2200K. 90s continuous air can be supplied during the tests [12].

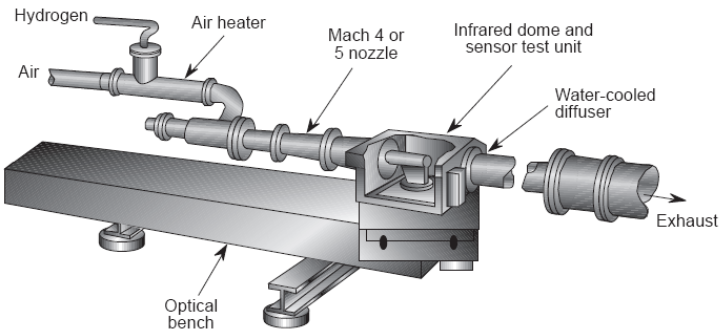

Figure 2.13 Schematic Representation of High Speed Aerothermal Sensor Test Setup

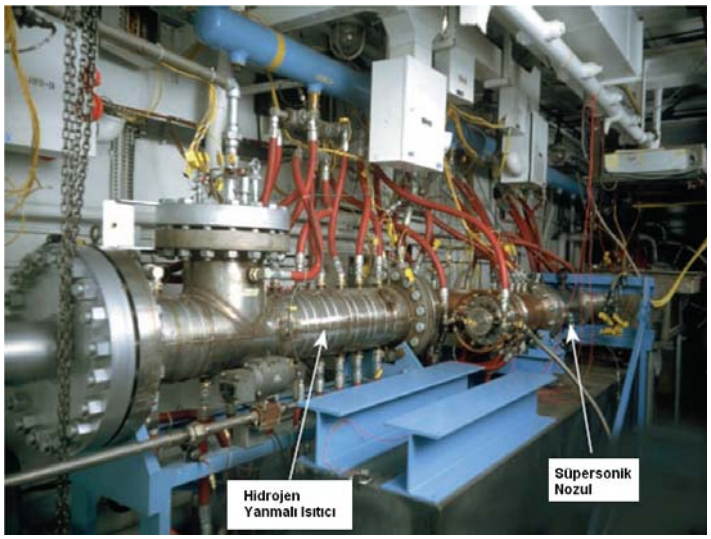

Figure 2.14 Vitiator of High-Speed Aerothermal Sensor Test Setup

2.11 DRDL Scramjet Combustor Test Setup

DRDL scramjet Combustor Test Setup has been built in India, Hyderabad DRDL Head Hypersonic Propulsion Division. The facility comprises a hydrogen fueled vitiator, axially symmetrical De-Laval nozzle and a circular to rectangular transition duct. Scramjet test setup is given in Figure 2.15. Vitiator can supply 1430K and 14.5Bar conditioned air. Air, oxygen and hydrogen mass flow rates are constant during the tests [13][14].

Figure 2.15 DRDL Test Setup

2.12 NASA Langley Mach 4 Scramjet Test Setup

NASA Langley Mach 4 Scramjet Test Setup (Combustion Heated Scramjet Test Facility-CHSTF) can simulate ramjet/scramjet engine air intake conditions. A hydrogen fueled vitiator is used in the setup and make up oxygen is given to the vitiator. Scheme of the test setup is given in Figure 2.16.

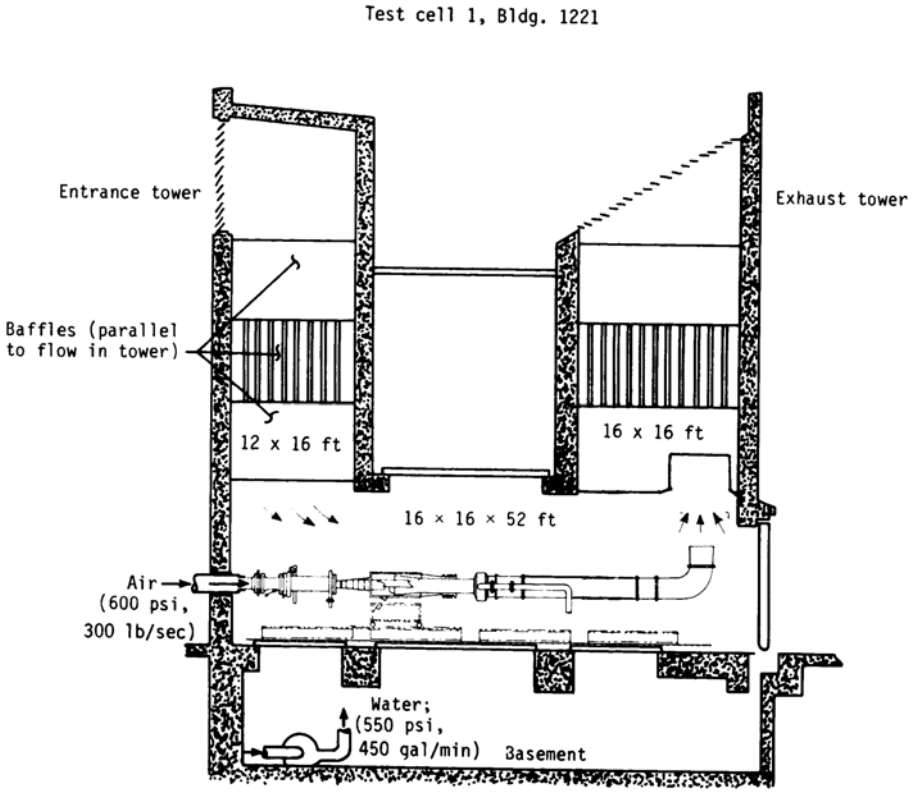

Figure 2.16 Langley Mach 4 TestSetup

Schematic representation of the vitiator is given in Figure 2.17. Oxygen is injected in the flow direction. This oxygen injection area is called as premixing zone. An injector plate is placed after the premixing zone. Hydrogen injectors cross the injector plate. A pilot flame igniter is used to start the combustion. It is known that the pressure and temperature limits of the vitiator are 13.1Bar and 1250K. But these limits were increased up to 41.4bar and 1666K with the recent modifications. Test setup can simulate Mach 4 and 8 conditions.

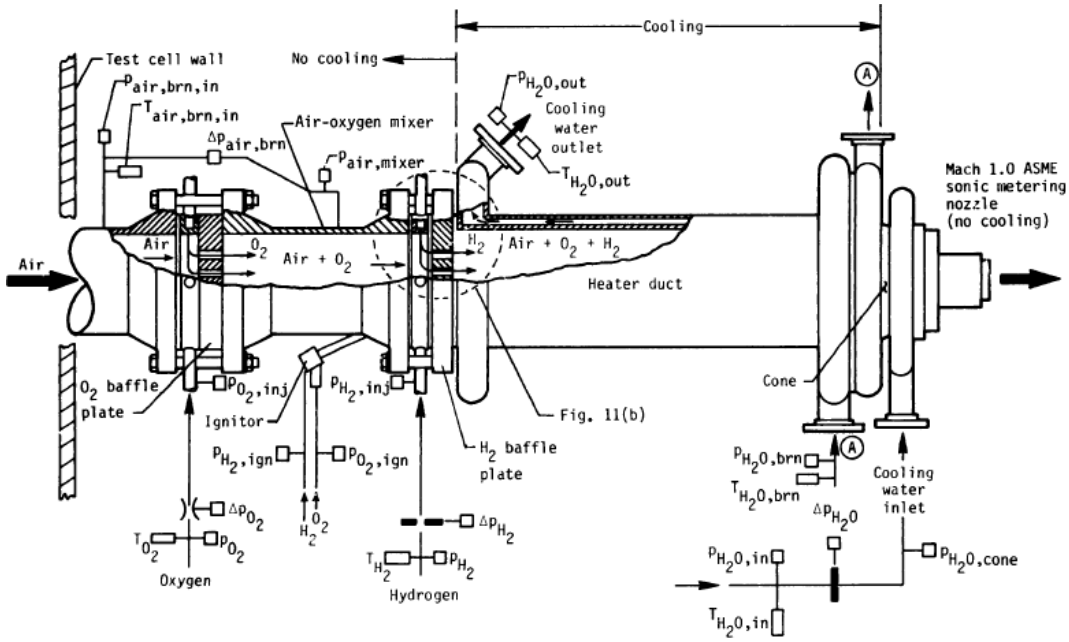

Figure 2.17 CHSTF Vitiator

2.13 TNO Prints Maurit's Direct Connect Test Setup

Solid Propellant Ramjet studies have been done in TNO Prints Maurit's Laboratory since 1989. Performance values of different kinds of ramjet propulsion system's are estimated in this test setup. Until 2000, experimental studies have been performed for the ramjet powered rockets (ram rocket). An image is given during a free jet test in Figure 2.18. In this test setup, pressurized hot air is given to the ramjet combustor under subsonic conditions. The enthalpy value is provided with the vitiator. [17]

The vitiator included test setup is shown in Figure 2.19. The ramrocket is located behind the free jet nozzle which attached to the tail of the vitiator [18]. Methane and hydrogen can be used as propellants for the vitiator. Make up oxygen is given to the vitiator. The maximum total temperature 1500K, the maximum total pressure 60Bar and mass flow rates changes from 0.25 to 10kg/s. Test duration may be up to 30s. Schematic vitiator is given in Figure 2.20.

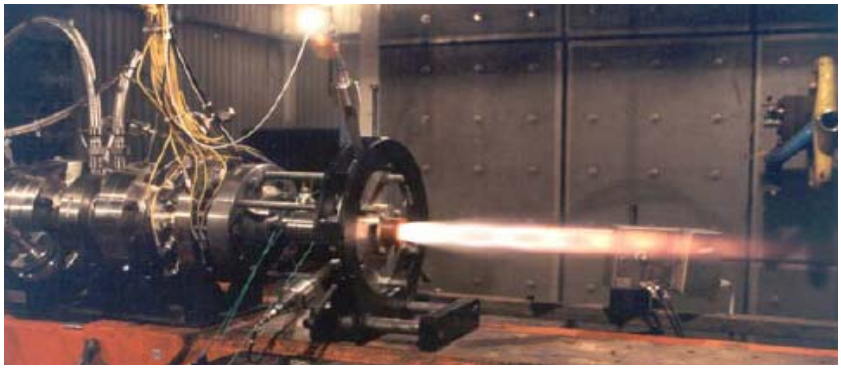

Figure 2.18 Solid Fuel Ramjet Motor Test on TNO Test Stand

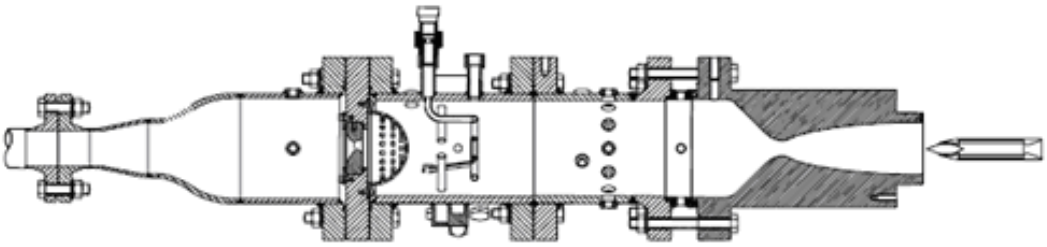

Figure 2.19 Schematic Representation of the Free Jet Test Setup

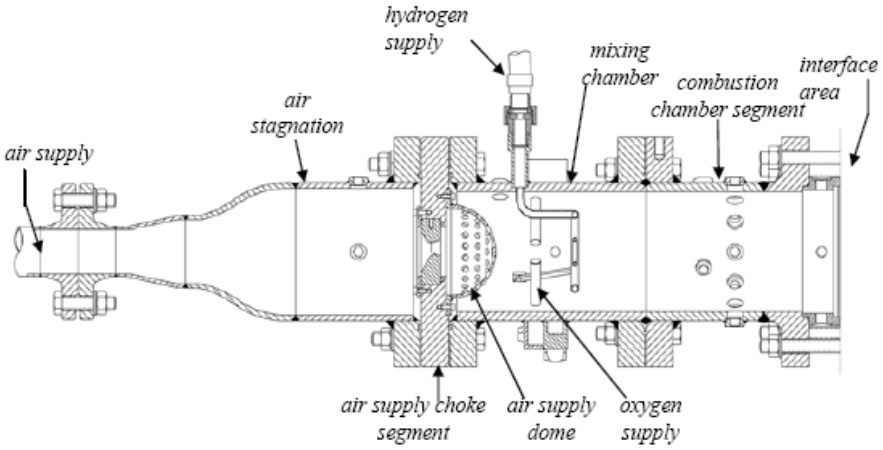

Figure 2.20 TNO Vitiator

TNO vitiator consist a stagnation zone and a combustion zone. Air comes to the stagnation zone from a sonic orifice which allows measuring the mass flow rate. There is a dome after the orifice which allows distributing the air uniformly

through the combustion chamber. Two sets of oxygen and hydrogen injectors exist. Two sets injectors ensure good mixing and enough size of flame front. It is known that ignition has been started by pyrotechnique methods until 1996. Nowadays a methane/oxygen pilot flame igniter is used for ignition. This igniter is also used for controlling the temperatures in the combustion chamber. The igniter products may be changed to improve the ignition. [17]

There are 12 thermocouples at the end of the combustion chamber. Thermocouples are located to measure proper temperature values and the measurement results are shown in Figure 2.21. It is understood that combustion is stable an temperature distribution at the end of the vitiator is homogenous.

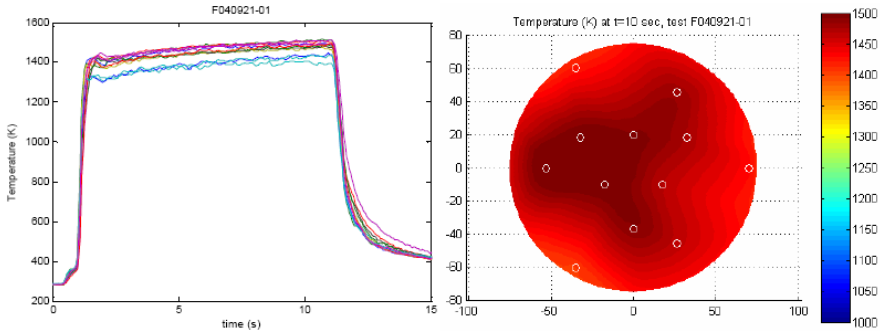

Figure 2.21 Exit Temperature Distribution of TNO Vitiator

To increase the life of the vitiator and facilitate changing of the injectors, vitiator has been manufactured by better thermal characteristic materials. Oxygen injectors were replaced with more compact ones. Secondary hydrogen injector which behaved as a flame arrestor was removed from the vitiator. Mass flow rate capacity of hydrogen was increased to design value. With these modifications, vitiator can produce air up to 1500K and 5kg/s [17].

2.14 GASL Accelerated Flight Simulation Test Setup

General Applied Science Laboratory (GASL) test setup includes sea level and Mach 3-4 test capability under vacuum conditions. Ramjet, scramjet and rocket engines can be tested in the facility. Air vitiator used in the GASL is shown in Figure 2.22. In the vitiator, the total enthalpy values can be changed by tuning hydrogen quantity. Replenishment oxygen is given to the vitiator and O2 molar ratio is kept as %21. [18]

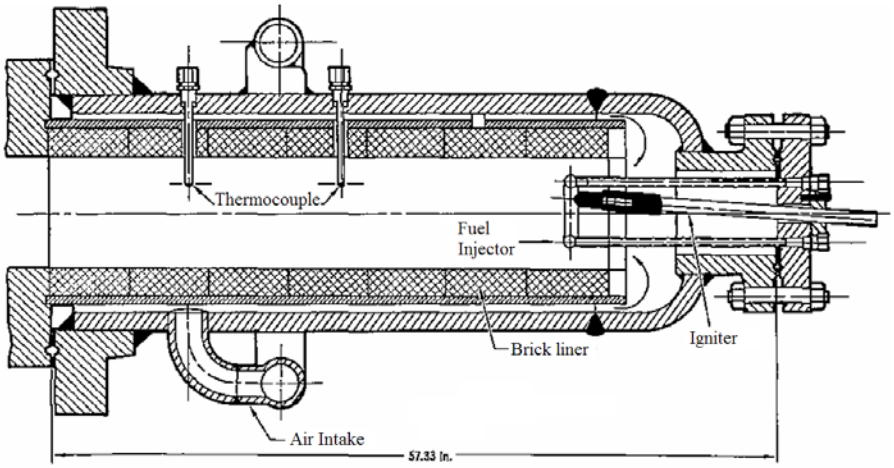

Figure 2.22 GASL Air Heater

2.15 The Atlantic Research Corporation-ARCF

As from 1980, Atlantic Research Corporation makes Ramjet flight simulations in Connected Pipe Ramjet test setup in Virginia. Especially gas generator ramjet tests are performed in this facility. The conditions from sea level Mach 2 to 18000m Mach 4 can be simulated in this facility. 0.9-13.6kg/s mass flow rate, 17Bar and 2500K total condition air can be supplied to the test unit.

Schematic representation of the test set up is given in Figure 2.23 [19]. Propane is preferred as fuel for the vitiator. Propane is given into the vitiator in flow direction. Pyrophoric Tri-ethyl-borane is used for ignition.

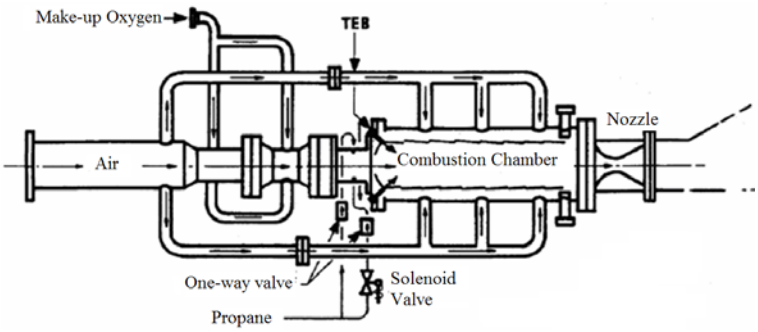

Figure 2.23 Shematic Representation of ARC Test Setup

Table 2.1 Important Operational Vitiators in the World

	Propellant	**Total Pressure**	**Total Temperature**	**Mass Flow Rate**
WPAFB	JP—7, H_2 Ethylene	52	923	13.6
NAVAL PGS	Hydrogen	—	845	3.63
NASA Langley DCSCTF	Hydrogen	8-35	889—2111	0.45-13.6
NASA 8-Foot	Methane	—	2027	—
AEDC, APTU	Butane	—	2500K	—
UTRC	Hydrogen	—	2222	
CAOS	Hydrogen	45	1200—2000	2
John Hopkins AATDL	Hydrogen	17-69	2222	—
DRDL	Hydrogen	14.5	1430	
NASA Langley Mach 4 (CHSTF)				
TNO—Prints Maurits	Methane / Hydrogen	60	1150	0.25—10
GASL	Hydrogen	—	4500	22
ARCF	Propane	17	2500	0.9—13.6

CHAPTER 3

COMBUSTION BACKGROUND

3.1 Introduction to Combustion

Combustion is perhaps described most simply as an exothermic reaction of a fuel and oxidant [20]. Rankine-Hugoniot (RH) relations show that two classes of waves can propagate in a combustible mixture, namely subsonic deflagration waves and supersonic detonation waves [21]. Figure 3.1 illustrates schematically a long tube containing a premixed combustible gas mixture. If the combustible gas mixture is ignited at the left end of the tube, a planar combustion wave propagates to the right into the unburned reactants, leaving the burned products behind the wave [22].

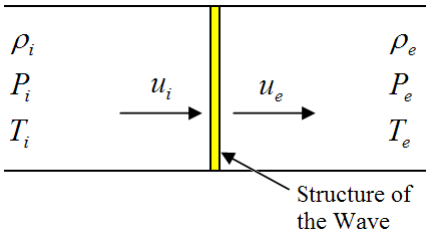

Figure 3.1 Open End Steady Combustion Wave

Table 3.1 General Characteristics of Detonation and Deflagration Waves

	Deflagration	**Detonation**
$\mathbf{M_1}$	< 1	> 1
$\mathbf{M_2}$	< 1	≤ 1
$\mathbf{V_2/V_1}$	> 1	< 1
$\mathbf{P_2/P_1}$	< 1	> 1
$\mathbf{T_2/T_1}$	< 1	> 1

Whether a deflagration wave or detonation wave occurs in a given situation depends on several variables, but the principle factors are the composition of the gaseous reactants, and whether the tube is open or closed at the ignition [22]. The items at prime interest in studying combustion waves are the wave propagation speed and the flow properties of the products of combustion. For a deflagration wave, the wave propagation speed is termed the ***flame speed***, and for a detonation wave is termed the ***detonation velocity***. Combustion is the study of chemically reacting flows with rapid, highly exothermic reactions. It is interdisciplinary in nature, comprising thermodynamics, chemical kinetics, fluid mechanics and transport phenomena [24].

3.2 Thermodynamics of Combustion

Combustion is an oxidation process and is usually exothermic (i.e. releases the chemical energy contained in a fuel as thermal energy). The most common combustion process encountered in engineering are those which convert a hydrocarbon fuel into carbon dioxide and water. This kind of combustion is usually performed using air because it is freely available in nature.

The model used in this thesis presupposes that combustion is a process that can take place in only one direction and it ignores the true statistical nature of chemical change. Combustion is the combination of various atoms and molecules and takes place when they are close enough to interact, but there is also the possibility of atoms which have previously joined together to make a product molecule separating to form reactants again. The whole mixture is really taking part in a molecular "barn dance" and the tempo of the dance is controlled by the temperature of the mixture. The process of molecular breakdown is referred to as dissociation. In reality a true combustion process is even more complex than this because the actual rate at which the reactions can occur is finite. This rate is the basic cause of some of the pollutants produced by the engines. In fact, in most combustion processes the situation is even more complex because there is an additional factor

affecting combustion, which is related to the rate at which the fuel and air can mix [24].

The various different types of combustion processes are listed in Table 3.2 and some examples are given of where the processes might be found. In this thesis our combustion process will be based on equilibrium thermodynamics, and will cover combustion processes without "*dissociation*". It will be found that equilibrium thermodynamics enables a large number of calculations to be performed. It does not allow the calculation of pollutants.

3.3 Extensive and Intensive Properties

The numerical value of an "extensive property" depends on the amount (mass or number of moles) of the substance considered. Extensive properties are usually denoted with capital letters; for example, V(m^3) for volume, etc. On the other hand, an intensive property is expressed per unit mass (or per mole), and its numerical value is independent of the amount of substance present. Mass-based intensive properties are generally denoted with lower-case letter; for example υ (m^3/kg) for specific volume, etc [25]. Temperature T and pressure P are important exceptions to this lower-case convention. Molar based intensive properties are shown in over bar form e.g. $\overline{u}$. Extensive properties are obtained simply from the corresponding intensive properties by multiplying the property value per unit mass (or mole) by the amount of mass (or number of moles); i.e. [25].

$$V = m\upsilon \text{ or } (N\overline{\upsilon}) \qquad 3.1$$

Table 3.2 Factors Affecting Combustion Processes [24]

Conditions of Combustion	Classification	Examples
Time dependence	Steady	Gas turbine combustion chamber, boilers
	Unsteady	Petrol engine, diesel engine
Spatial Dependence	Zero-dimensional	For modeling purposes, well-stirred reactors
	One-dimensional	Approximated in pipe flows, flat flame burners
	Two-dimensional	Axisymmetric flames, e.g. Bunsen burner
	Three-dimensional	General Combustion
Mixing of initial reactants	Premixed	Petrol or spark ignition engines
	Non-premixed	Diesel engine, gas turbine combustion chamber
Flow	Laminar	Special cases for measuring flame speed
	Turbulent	Most real engine cases, boilers
Phase of reactants	Single	Spark ignited gas engines, petrol engines with fuel completely evaporated, gas-fired boilers
	Multi phase	Diesel engines, gas turbines, coal and oil fired boilers
Reaction sites	Homogenous	Spark-ignition engines
	Heterogeneous	Diesel engines, gas turbines, coal fired boilers
Reaction rate	Equilibrium chemistry (infinite rate)	Approached by some processes in which the combustion period is long compared with the reaction
	Finite rate	All real processes, causes many pollutant emissions
Convection conditions	Natural	Bunsen flame, gas cooker, central heating boiler
	Forced	Gas turbine combustion chamber, large boilers
Compressibility	Incompressible	Free flames
	Compressible	Engine flames
Speed of combustion	Deflagration	Most normal combustion processes
	Detonation	“Knock” in spark ignition engines, explosions

3.4 First Law of Thermodynamics

Fundamental principle of the first law of thermodynamics is conservation of energy. First law will be applied in this thesis for a control volume with fixed boundaries and steady flow which schematic representation of this model is given in Figure 3.2.

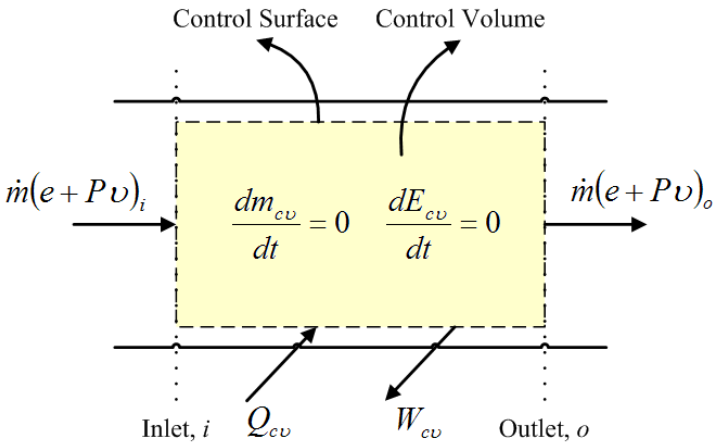

Figure 3.2 Control Volume with Fixed Boundaries and Steady Flow

The steady-state, steady flow (SSSF) form of the first law is particularly useful for our problem in this thesis. The SSSF first law is expressed as;

$$\dot{Q}_{CV} - \dot{W}_{CV} = \dot{m}e_o - \dot{m}e_i + \dot{m}(p_o\upsilon_o - p_i\upsilon_i) \qquad 3.2$$

$\dot{Q}_{CV}$	:	Heat transfer rate across the control surface from the surroundings, to the control volume
$\dot{W}_{CV}$	:	Work rate done by the control volume, including shaft work, but excluding flow work
$\dot{m}e_o$	:	Energy rate coming out of the control volume
$\dot{m}e_i$	:	Rate of energy coming into the control volume
$\dot{m}(p_o\upsilon_o - p_i\upsilon_i)$	:	Net work rate done by flow

Principle assumptions used in this relation are given as follows [25]:

- The control volume is fixed to the coordinate system.
- The properties of the fluid at each point within the control volume, or on the control surface, do not vary with time.
- Fluid properties are uniform over the inlet and outlet flow areas.
- There is only one inlet and one exit flow.

The specific energy e and of the inlet and outlet streams consists of the specific internal, kinetic and potential energies, i.e.,

$$e = u + \frac{1}{2}V^2 + gz \tag{3.3}$$

Here we introduce the enthalpy, h;

$$h \equiv u + P\upsilon = u + \frac{P}{\rho} \tag{3.4}$$

Combining Equation 3.2 and 3.3 with Equation 3.4; it is obtained

$$\dot{Q}_{CV} - \dot{W}_{CV} = \dot{m}\left[(h_o - h_i) + \frac{1}{2}\left(V_o^2 - V_i^2\right) + g(z_o - z_i) \right] \tag{3.5}$$

Equation 3.5 can be defined on a mass specific basis as follows;

$$q_{CV} - w_{CV} = (h_o - h_i) + \frac{1}{2}\left(V_o^2 - V_i^2\right) + g(z_o - z_i) \tag{3.6}$$

3.5 Stoichiometry

The stoichiometric quantity of oxidizer is just that amount needed by completely burn a quantity of fuel. If more than a stoichiometric quantity of oxidizer is supplied, the mixture is said to be lean, while supplying less than the stoichiometric oxidizer results in a rich mixture. The stoichiometric oxidizer-fuel ratio is

determined by atomic balance, assuming that the fuel reacts to form an ideal set of products. For a hydrocarbon fuel reacting with air given by C_xH_y, the stoichiometric relation can be expressed as [19]

$$C_xH_y + a(O_2 + 3.76N_2) \rightarrow xCO_2 + (y/2)H_2O + 3.76aN_2 \quad 3.7$$

The stoichiometric air-fuel ratio can be found as[25];

$$(A/F)_{stoic} = \left(\frac{\dot{m}_{air}}{\dot{m}_{fuel}}\right)_{stoic} = \frac{4.76a}{1} \times \frac{MM_{air}}{MM_{fuel}} \quad 3.8$$

where MM_{air} and MM_{fuel} molecular mass of the air and fuel respectively.

The equivalence ratio, ϕ, is commonly used to indicate quantitatively whether a fuel-oxidizer mixture is rich, lean or stoichiometric. The equivalence ratio is defined as

$$\phi = \frac{(A/F)_{stoic}}{(A/F)} = \frac{(F/A)}{(F/A)_{stoic}} \quad 3.9$$

If ϕ<1 than mixture is lean, ϕ=0 than mixture is stoichiometric, ϕ>1 than mixture is rich. In many combustion applications, ϕ, is the single most important factor in determining a system's performance [19].

3.6 Absolute or standardized Enthalpy and Enthalpy of Formation

In dealing with chemically reacting systems, the concept of absolute enthalpies is vitally important. For any species, we can define an absolute enthalpy that is the sum of an enthalpy that takes into account the energy associated with chemical bonds, the enthalpy of formation, h_f, and an enthalpy that is associated only with

the temperature, the sensible enthalpy change , Δh_s. Thus, we can write the molar absolute enthalpy for species;

$$\overline{h}_i(T) = h_{f,i}(T_{ref}) + \left(\overline{h}_i(T) - \overline{h}^o_{f,i}(T_{ref})\right) \quad 3.10$$

$$\Delta\overline{h}_{s,i}(T) = \overline{h}_i(T) - \overline{h}^o_{f,i}(T_{ref}) \quad 3.11$$

For this study standard reference temperature T_{ref} and standard reference pressure P_{ref} are assumed 25°C and 1atm respectively consistent with the NASA SP 3001 Thermochemistry Data Base which is given in **Hata! Başvuru kaynağı bulunamadı.**. Enthalpies of formation of the elements in their naturally occurring state at the reference state temperature and pressure are zero.

3.7 Enthalpy of Combustion

Consider the steady flow reactor shown in Figure 3.3, in which a stoichiometric mixture of reactants enters and products exits, both at standard state conditions. It is assumed that the combustion process is completed. For the products to exit at the same temperature as the entering reactants, heat must be removed from the reactants. The amount of heat removed can be related to the reactant and product absolute enthalpies by applying the first law for steady flow.

$$q_{CV} = h_o - h_i = h_{prod} - h_{reac} \quad 3.12$$

$$\Delta h_R = q_{CV} = h_{prod} - h_{reac} \quad 3.13$$

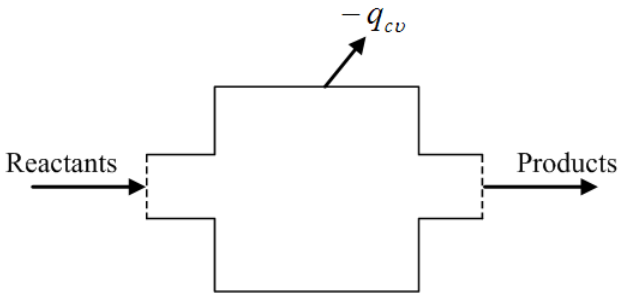

Figure 3.3 Steady Flow Reactor

In a combustion process when the work interactions, kinetic and potential energy changes were neglected, the released chemical energy is given to the surrounding with heat transfer or stays in the system and increase the temperature of the combustion products. The less the heat transfer to the surrounding the more high temperature of the combustion products. When there is no heat transfer to the surrounding ($q_{CV} = 0$), the temperature of the combustion products reach the highest level. This temperature is called as "*adiabatic flame temperature*" of the reaction or "*adiabatic combustion temperature*". Two different adiabatic flame temperatures are defined:

- Adiabatic flame temperatures for constant pressure combustion
- Adiabatic flame temperatures for constant volume combustion

We deal with a constant pressure system, which is appropriate in dealing with a vitiator.

If a fuel-air mixture burns adiabatically at constant pressure, the absolute enthalpy of the reactants at the initial state (say $T = T_i, P = P_i$) equals the absolute enthalpy of the products at the final state ($T_{ad} = T_o, P_o = P_i$), i.e.

$$H_{react}(T_i, P) = H_{prod}(T_{ad}, P) \qquad 3.14$$

or frequently on a per-mass-of-mixture basis,

$$h_{react}(T_i, P) = h_{prod}(T_{ad}, P) \tag{3.15}$$

where Equation 3.15 defines constant pressure adiabatic flame temperature.

3.8 The Rates of Reactions and Temperature Dependency of Rate

All chemical reactions, whether of the decomposition or combustion type, take place at a definite rate and depend on the conditions of the system. The most important of these conditions are the concentration of the reactants, the temperature, radiation effects, and the presence of a catalyst or inhibitor. Reaction rate may be defined in terms of the concentration of any of the reactants or any products; i.e., the rate may be expressed as the decreasing rate of the concentration of a reactant or vice versa. A stoichiometric relation describing a one-step chemical reaction of arbitrary complexity can be represented by the Equation 3.16 [23]

$$\sum_{j=1}^{n} \nu'_j M_j = \sum_{j=1}^{n} \nu''_j M_j \tag{3.16}$$

ν'_j	:	The stoichiometric coefficient of the reactants
ν''_j		The stoichiometric coefficients of the products
M		An arbitrary specification of all chemical species
n		The total number of species involved

ν_j of M_j equals zero if a species represented by M_j does not occur as a reactant or product. The law of mass action states that the rate of disappearance of a chemical species i, defined as RR_i, is proportional to the product of the concentrations of the reacting chemical species, which is experimentally confirmed. Each concentration raised to a power equal to the corresponding stoichiometric coefficient, i.e.,

$$RR_i \propto \prod_{j=1}^{n} \left(M_j\right)^{\nu'_j} \;,\; RR_i = k \prod_{j=1}^{n} \left(M_j\right)^{\nu'_j} \qquad 3.17$$

where k is the specific reaction rate coefficient. In Equation 3.16 n is called the overall order of the reaction; ν'_j itself would be the order of the reaction with respect to species j. In an actual reacting system, the rate of change of the concentration of a given species i is given by

$$\frac{d\left(M_i\right)}{dt} = \left[\nu''_i - \nu'_i\right] RR = \left[\nu''_i - \nu'_i\right] k \prod_{j=1}^{n} \left(M_j\right)^{\nu'_j} \qquad 3.18$$

since ν''_i moles of M_i are formed for every ν_i moles of M_i consumed. The use of this complex representation prevents error in sign and eliminates confusion when stoichiometric coefficients are different from one [23].

In many systems M_i can be formed not only from a single-step reaction such as that represented by Equation 3.18, but also from many different such steps leading to a rather complex formulation of the overall rate. However, for a single-step reaction such as 3.18, $\sum \nu_i$ not only represents the overall order of the reaction, but also the molecularity, which is defined as the number of molecules that interact in the reaction step.

Generally the molecularity of most reactions of interest will be 2 or 3. For a complex reaction scheme the concept of molecularity is not appropriate and the overall order can take various values including fractional ones.

3.9 Arrhenius Rate Expression

Most chemical reactions that take place have their rates dominated by collisions of two species that may have the capability to react. Thus, most simple reactions are

second order. Other reactions are dominated by a loose bond breaking step and thus are first order. Most of these latter type reactions fall in the class of decomposition processes. According to Lindemann's theory of first-order processes, first-order reactions occur as a result of a two-step process [24]. An arbitrary second-order reaction may be written as

$$A + B \rightarrow C + D \tag{3.19}$$

where a real example would be the reaction of oxygen atoms with nitrogen molecules

$$O + N_2 \rightarrow NO + N \tag{3.20}$$

For the arbitrary reaction (Equation 3.19), the rate expression takes the form

$$RR = \frac{d\overline{A}}{dt} = -k\overline{A}\,\overline{B} = -\frac{d\overline{C}}{dt} \tag{3.21}$$

Specifying the reaction in the manner above does not mean every collision of the reactants A and B would lead to products or cause the disappearance of an amount of either. Arrhenius propose a simple theory that accounts for this fact and gives a temperature dependency of k. Arrhenius stated that only molecules that have energy greater than a certain amount E will react. Molecules get the additional energy necessary from collisions induced by the thermal condition that exists. These high-energy activated molecules lead to products. Arrhenius' postulate may be written as

$$RR = Z_{AB} \exp(-E/RT) \tag{3.22}$$

Z_{AB} : Gas kinetic collision frequency
$\exp(-E/RT)$: Boltzmann factor

Kinetic theory shows that the Boltzmann factor gives the fraction of all collisions that have an energy greater than E. The energy term in the Boltzmann factor may be considered as the size of the barrier along a potential energy surface for a system of reactants going to products and is represented schematically in Figure 3.4. The state of the reacting species at this activated energy can be thought of as some intermediate complex that leads to the products. This energy is referred to as the activation energy of the reaction and is generally given the symbol E_A. In Figure 3.4, this energy is given as the symbol E_f to distinguish it from the condition in which the product species can revert to reactants by a backward reaction. The activation energy of this backward reaction is represented by E_b, and is larger than E_f. Exothermic condition for reactants going to products is shown in Figure 3.4. In most cases the more exothermic a reaction is, the smaller the activation energy.

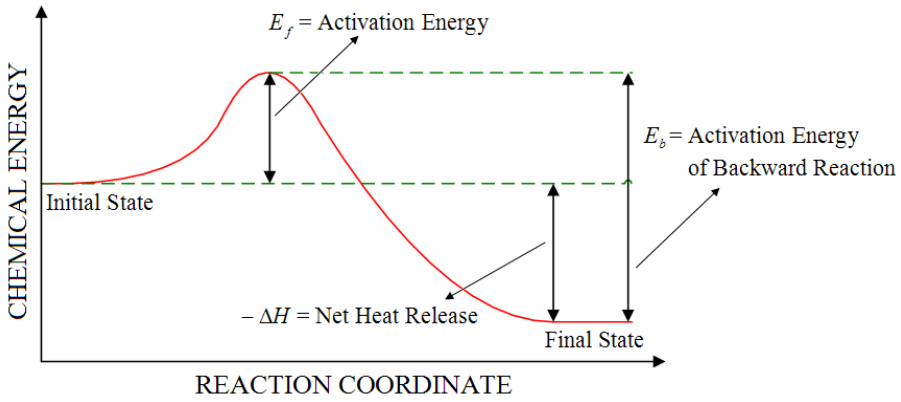

Figure 3.4 Energy as a Function of a Reaction Coordinate for a Reacting System

Considering again Equation 3.22 and referring to E as an activation energy, attention is focused on the collision rate Z_{AB}, which from simple kinetic theory can be represented by [23]

$$Z_{AB} = (A)(B)\sigma_{AB}^2 [8\pi k_B T / \mu]^{1/2} \qquad 3.23$$

where σ_{AB} is the hard sphere collision diameter, k, the Boltzmann constant, μ the reduced mass $m_A m_B/(m_A + m_B)$ and m the mass of the species. Z_{AB} may be written in the form

$$Z_{AB} = Z'_{AB}(A)(B) \tag{3.24}$$

Thus, the Arrhenius form for the rate is

$$RR = Z'_{AB}(A)(B)\exp(-E/RT) \tag{3.25}$$

When compared to the reaction rate written from the law of mass action, it can be found that

$$k = Z'_{AB}(A)(B)\exp(-E/RT) = Z''_{AB}T^{1/2}\exp(-E/RT) \tag{3.26}$$

Thus, the important conclusion is that the specific reaction rate constant k is only dependent on temperature. Actually, when complex molecules are reacting, not every collision has the proper steric orientation for the specific reaction to take place. To include the steric probability k is written as

$$k = Z''_{AB}T^{1/2}\exp(-E/RT)\wp \tag{3.27}$$

where $\wp$ is a steric factor, which at times can be a very small number. Most generally, however, the Arrhenius form of the reaction rate constant is written as

$$k = \text{const}\,T^{1/2}\exp(-E/RT) = A\exp(-E/RT) \tag{3.28}$$

where the constant A takes into account the steric factor and the terms in the collision frequency other than the concentrations and is referred to as the "*kinetic pre-exponential A factor"*. The factor A is proportional with $T^{1/2}$. Equation 3.28 permits convenient straight line correlations of data on $\ln k$ versus $(1/T)$ plots.

Data that correlate as a straight line on a $\ln k$ versus $(1/T)$ plot are said to follow Arrhenius kinetics, and plots of the logarithm of rates or rate constants as a function of $(1/T)$ are referred to as Arrhenius plots. The slope of this line is equal to $(-E/R)$ and thus the activation energy may be determined readily. Low activation energy processes proceed faster than high activation energy processes at low temperatures and have much less temperature sensitivity. At high temperatures, high-activation energy reactions can prevail, because of this temperature sensitivity [21]. Methane combustion is exothermic reaction and activation energy is small. There is no decomposition if it is used according to the specification. No dangerous decomposition products known for Methane. Methane may form explosive gas mixtures with air [33].

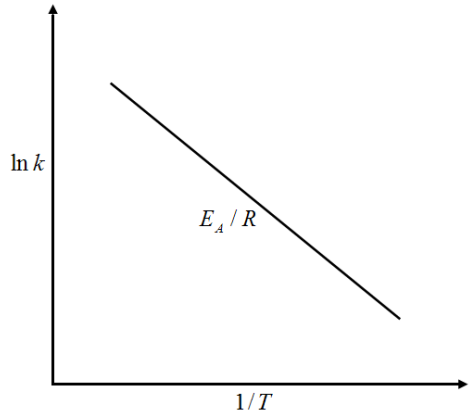

Figure 3.5 Arrhenius Plot of the Specific Reaction Rate Constant as a Function of the Reciprocal Temperature

3.10 High Temperature Oxidation of Methane

Methane exhibits certain oxidation characteristics that are different from all other hydrocarbons. Tables of bond energy list the first broken C-H bond in methane to be kilocalories more than the others, and certainly more than the C-H bonds in longer-chain hydrocarbons. Thus, it is not surprising to find various kinds of experimental evidence to lead one to believe that it is more difficult to ignite methane/air (oxygen) mixtures than it is with other hydrocarbons. Oxidation

mechanism of the Methane is divided in two groups as high temperature and low temperature oxidation. Low temperature oxidation is out of the concept of this thesis. At high temperatures the thermal decomposition of the methane provides the chain initiation step [23], namely

$$CH_4 + M \rightarrow CH_3 + H + M \qquad 3.29$$

The methyl radical then combines with an oxygen atom to form formaldehyde (CH2O); the formaldehyde, in turn, is attacked by OH, H, and O radicals to produce the formyl radical (HCO); the formal radical is converted to CO by a trio of reactions; and, finally, CO is converted to CO2, primarily by reaction with OH [19].

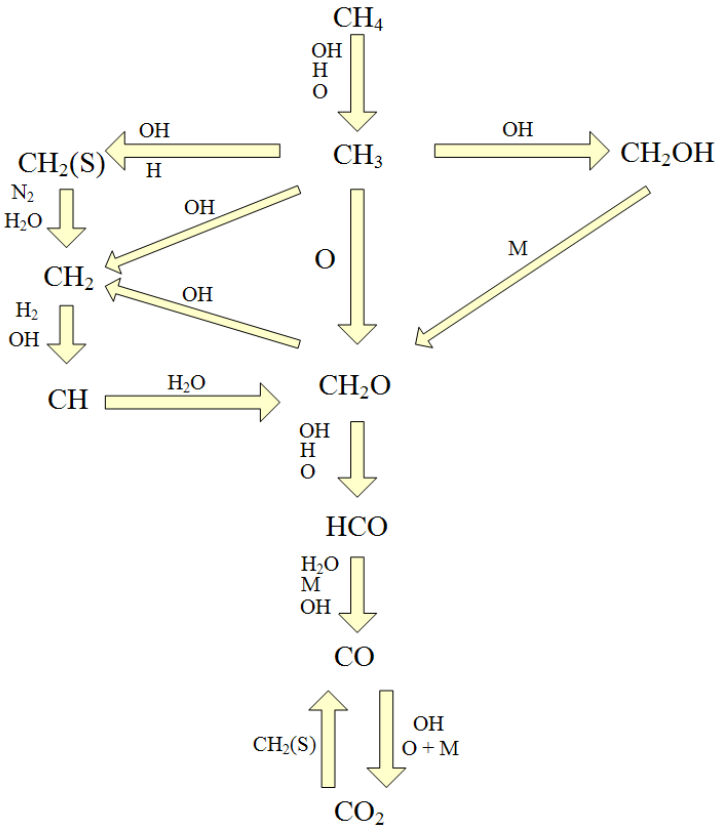

Figure 3.6 Major Reaction Paths for the High Temperature Oxidation of Methane

3.11 Models Used in Reactive Flow CFD Analyses

In practical devices turbulent flows are more frequently encountered than laminar flows. This fact is valid especially for gas turbine combustors. Unfortunately, the mathematical description of a turbulent flow and the solution is very difficult. Analytical and numerical solutions to turbulent flows are engineering approximations, even for the simplest geometries, and can be subject to large errors.

In this thesis, $k-\varepsilon$ turbulent model is used as a turbulence model and Eddy Break-up combustion model is used as a combustion model where the necessary information can be found in [31] and [32] respectively.

There are four flame types typically exist in combustion processes: where the related physical systems can be seen from Table 3.2.

1. Laminar Diffusion Flame
2. Laminar Premixed Flame
3. Non-premixed Turbulent Flame
4. Turbulent Premixed Flame

Non-premixed turbulent flame is arisen in a gas turbine combustion chamber and it is taken into account in this thesis. More detailed information about the non-premixed turbulent flame can be found in [21],[23],[25].

CHAPTER 4

DESIGN OF THE VITIATOR

In this chapter design of the vitiator is explained. As a first, a thermodynamic model of air heater is constituted. A Combustion Chamber Design Code (CCDC) is and the modules of the CCDC are introduced. The design parameters are explained clearly in this section. Finally heater design is given at the end.

4.1 Thermodynamic Model of Air Heater

A thermodynamic model is necessary to design a combustion chamber. Design parameters and the other necessary input parameters of the combustion chamber can be decided in this way. After construction the thermodynamic model the amount of the required fuel and oxidizer can be found easily. Also a thermodynamic model can be used as a design guideline because model calculations limit the design. It means the model exhibits if the necessary conditions are ensured or not.

Heater is treated as a control volume with fixed boundaries and steady flow which schematic representation of this model is given in Figure 4.1. Conservation of energy equation in this system is given as follows.

$$\dot{Q} - \dot{W} = \sum \dot{n}_o \left(\bar{h}_f^o + \bar{h} - \bar{h}^o \right)_o - \sum \dot{n}_i \left(\bar{h}_f^o + \bar{h} - \bar{h}^o \right)_i \qquad 4.1$$

Absolute enthalpy of the reactants and the products are the same as explained in chapter 3.7. While solving combustion problems, it is easier to study with the equations for unit mole. By dividing each term with fuel mole number in Equation

4.1, Equation 4.2 can be derived easily [6]. This is the equation of conservation of energy for the combustion of one mole fuel.

$$Q - W = \sum n_o \left(\bar{h}_f^o + \bar{h} - \bar{h}^o \right)_o - \sum n_i \left(\bar{h}_f^o + \bar{h} - \bar{h}^o \right)_i \qquad 4.2$$

$\dot{n}_o$	:	Mole number of the combustion products	mol/s
$\dot{n}_i$	:	Mole number of the combustion reactants	mol/s
$\bar{h}_f^o$	:	Enthalpy of formation at standard reference state	kJ/kgK
$\bar{h}$	:	Sensible Enthalpy at given state	kJ/kgK
$\bar{h}^o$	:	Sensible Enthalpy at 25°C and 1atm	kJ/kgK

For simplicity Equation 4.2 can be expressed as follows.

$$Q - W = H_o - H_i \qquad 4.3$$

H_o	:	Total Enthalpy of the combustion products	mol/s
H_i	:	Total Enthalpy of the combustion reactants	mol/s

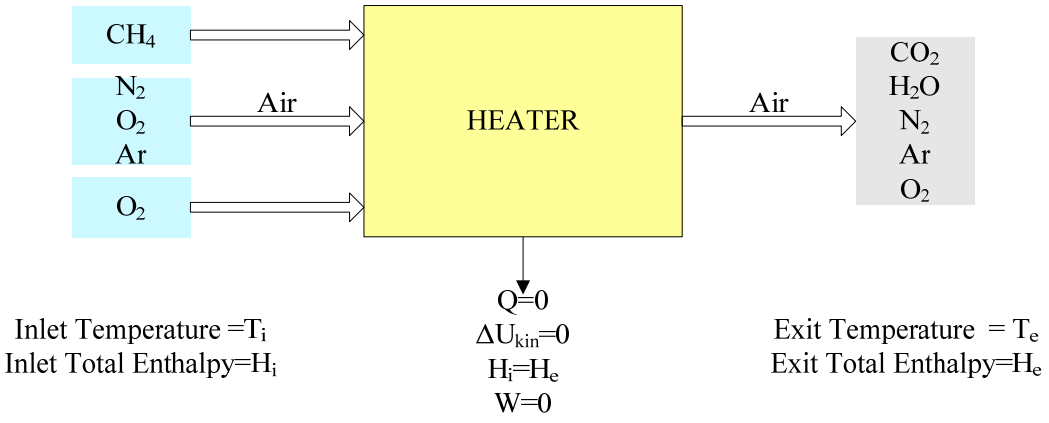

Figure 4.1 Thermodynamic Model of the Heater

For this model it is assumed that the combustion process is adiabatic and there is no kinetic energy change. The temperature augmentation of the air which heated by combustion process, come about by the internal energy alteration. At that rate it is

possible to say that the products total enthalpy is kept constant and equal to the reactants total enthalpy.

$$H_i = H_o \tag{4.4}$$

Complete combustion assumption is made in this model. Reactants of reaction are assumed as CH_4, N_2, O_2, Ar and the products CO_2, H_2O, N_2, Ar and O_2. Also it is necessary that the molar ratio of the oxygen of the entering air and heated air to be equal. Make up oxygen is given to the combustion chamber to maintain this requirement. If the states of the reactants are known, H_i can be easily found and vice versa for H_o. But it is not easy to calculate H_o on account of unknown values of the product temperatures. Consequently, if there are no analytical correlations which allow calculation of the sensible enthalpies of the products, adiabatic flame temperature must be found by trial and error [25].

4.2 Combustion Chamber Design Code (CCDC)

Heater is conceptually similar to a gas turbine engine combustion chamber (CC). There is not a known design procedures for the gas turbine CC. The combustion chambers are designed according to the empirical methods which were developed by the manufacturers in many years. During this thesis a certain amount of knowledge was compiled from the literature and a combustion chamber design code was generated. The modules of the CCDC are as follows;

- Combustion Module
- Combustion Chamber Design Module
- Swirler Design Module
- Injector Design Module
- Heat Transfer Module
- Pressure Loss Estimation Module

4.3 Combustion Module

The Combustion Module based on the thermodynamic model explained in Chapter 4.1. This module determines the necessary air, Methane and Oxygen quantities automatically after the user information entered to the input file. The working principle of the combustion module is as follows:

1. The necessary air quantity and air temperature is defined by the user.
2. Inlet temperatures of methane and oxygen are determined.
3. Using the NASA SP-3001 thermo chemistry database, the coefficient of a in Equation 4.6 is determined for 1 mole of air.
4. Finally the necessary Oxygen and Methane quantities are determined which bring up the temperature to the required level.

Following Equation is used to obtain necessary Methane and Oxygen quantities for a certain temperature hot air.

$$\begin{aligned}&(a)CH_4 + xO_2 + (0.2095O_2 + 0.7811N_2 + 0.0094Ar) \Leftrightarrow \\ &yCO_2 + zH_2O + wO_2 + 0.7811N_2 + 0.0094Ar\end{aligned} \qquad 4.5$$

When atomic balance rule was applied for the Equation 4.6, for a mole CH_4, while keeping the molar ratio of the oxygen constant, Equation 4.6 is obtained.

$$\begin{aligned}&(a)CH_4 + (2.7951a)O_2 + (0.2095O_2 + 0.7811N_2 + 0.0094Ar) \Leftrightarrow \\ &(a)CO_2 + (2a)H_2O + (0.7951a + 0.2095)O_2 + 0.7811N_2 + 0.0094Ar\end{aligned} \qquad 4.6$$

When Equations 4.4 and 4.6 were used to find the required Methane and Oxygen quantities, Figure 4.2 and Figure 4.3 can be derived easily. The feeding capacity of the heater can also be determined by means of these figures.

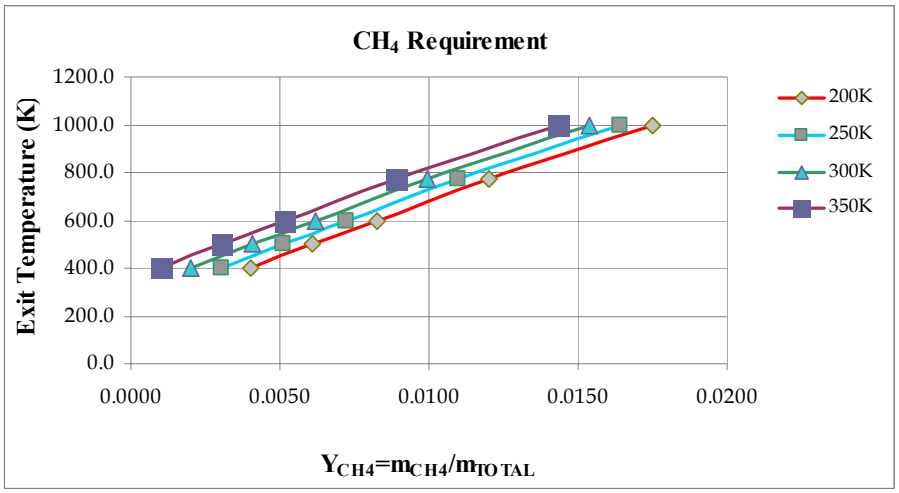

Figure 4.2 Heater CH_4 Requirements for Various Exit Temperatures

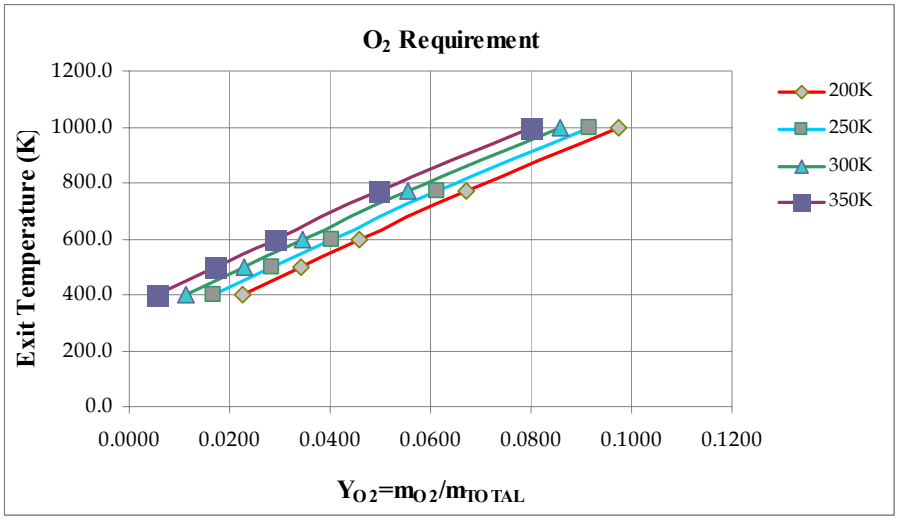

Figure 4.3 Replenishment O_2 requirements for Various Exit Temperatures

In a gas turbine combustion chamber, for a complete reaction, ϕ should be kept between 0.53-1.2 [20]. When the operating conditions of the air heater were considered, ϕ is about 0.2 and it is easy to see that ϕ is much less than 0.53. The lean combustion limit for Air-CH_4 is allowed as 0.25 [27]. It is also apparent that, heater operating conditions are below the lean combustion limit and it is difficult to achieve stable combustion at that point.

Incoming air was divided in two parts as combustion air and cooling air to achieve a stable combustion. The combustion air is directly taken into the CC liner and let react with the CH_4 in the liner. Cooling air is sent around the liner, between the liner and cooling jacket as shown in Figure 4.4. Cooling air has two main functions: to cool the combustion chamber and to decrease the high temperature at the end of the CC (similar to dilution air as in the gas turbine combustion chambers). Combustion chamber is cooled by cooling air via film cooling technique. Discharge coefficient was taken into account while choosing the cooling air hole diameters.

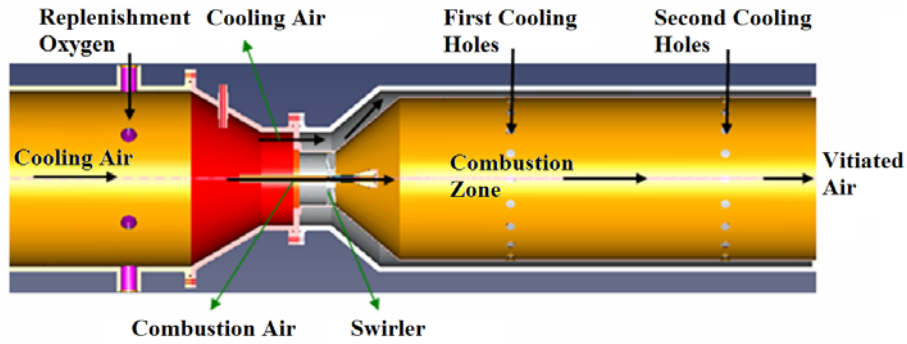

Figure 4.4 Conceptual Image of the Heater

Combustion chamber is divided in two sections namely primary zone and secondary zone. Primary zone is the region up to first cooling holes. There becomes strong recirculation zone. This is the most important zone for the combustion chamber because this is the region where the fuel and air mixed and almost the combustion completed.

When cooling air is sent around the liner, ϕ becomes nearly 0.6 in the liner. Stable combustion can be obtained in the chamber in this way. Cooling holes are opened around the liner which allows the cooling excess air penetrate through the liner. The input/output parameters of the Combustion Module are given in Table 4.1.

Table 4.1 Input and Output Parameters of Combustion Module

Input Parameters		Output Parameters
Inlet Temperature of air	:	Mass Flow Rate of Cooling Air
Inlet Temperature of CH_4	:	Mass Flow Rate of Combustion Air
Replenishment Oxygen Temperature	:	Required Mass Flow Rate of CH_4
Outlet Temperature of the Products	:	Required Mass Flow Rate of O_2
Total Mass Flow Rate	:	
Equivalence Ratio	:	

4.4 Combustion Chamber Liner Sizing Module

Combustion Loading Parameter (CLP) and Mach number in the combustion chamber are the most important design parameters. CLP reflects the influence of the most important parameters affecting combustion flame stability, namely, mass flow rate of air, volume of combustor and static pressure. CLP is defined as in Equation 4.7 and for maximum combustion efficiency in the CC liner, its value taken as 1.[28] The important parameter which affects the CLP thus the size of the CC liner is "Pressure Exponent-n". For hydrocarbon fuels n is taken as 1.8. Mass flow rate-$\dot{m}$ and the pressure value-P are determined according to the operating conditions. The CC volume V is calculated by the known values of n, P and $\dot{m}$. CC liner diameter can be calculated by the known volume and Mach number in the CC chamber liner. Average temperature is used for the calculations in the combustion chamber. Average temperature is defined as in Equation 4.8. Cooling air cuts across through the "Cooling Air Holes-CAH". The number and the diameter of the CAH are calculated with Equations 4.9 to 4.14.

$$CLP = \frac{\dot{m}}{P^n \times V} \tag{4.7}$$

$$T_{avg} = \frac{T_i + T_e}{2} \tag{4.8}$$

$\dot{m}$	:	Total mass flow rate through the liner	kg/s
P	:	CC Pressure	atm
V	:	CC liner Volume	m^3
n	:	Pressure Exponent (n =1.8 for hydrocarbons)	
CLP	:	Combustion Loading Parameter	

$$\dot{m} = (\pi / 4) n \times d^2 \times \rho \times U \quad 4.9$$

$$U = (2\Delta P / \rho)^{0.5} \quad 4.10$$

$$\rho = P / RT \quad 4.11$$

$$\dot{m} = (\pi / 4) \times n \times d^2 \times (2\Delta P \times \rho)^{0.5} \quad 4.12$$

$$n \times d^2 = 15.25 \times \dot{m} \times (P \times \Delta P / T)^{0.5} \quad 4.13$$

$$d_h = d / C_d^{0.5} \quad 4.14$$

$\dot{m}$	:	Total mass flow rate cutting across the holes	kg/s
ρ	:	Density	kg/m^3
ΔP	:	Pressure difference between the cooling annulus and CC liner	Pa
P	:	Pressure of the Cooling Air	Pa
n	:	Number of the CAH's	—
d	:	Diameter of the CAH	m
U	:	Velocity through the CAH	m/s
R	:	Gas Constant	kj/kgK
T	:	Combustion Chamber Temperature	K
d_h	:	Hydraulic Diameter of the CAH	m
C_d	:	Discharge Coefficient	—

Liner Sizing Module Input/Output Parameters are given in Table 4. 2. Another important sizing criterion of the CC liner is Divergence Angle (DA) which will be investigated in detailed to further sections.

Table 4. 2 Input and Output Parameters of the CCDC

Input Parameters		**Output Parameters**
Mach Number in the CC	:	
Mass Flow Rate of Combustion Air	:	
Necessary Methane Mass Flow Rate	:	CC Length
CC Pressure	:	CC Diameter
Inlet Temperature of the Air	:	Diameter of the Cooling Holes
CLP	:	
Pressure Exponent	:	
Cooling Hole Number	:	

4.5 Swirler Design Module

Swirler is a part which creates a toroidal flow in the CC and thus tends to be a flame holding mechanism. This toroidal flow triggers an extremely mixed flow. Mixing means high turbulence intensities and the higher turbulence intensity the more effective combustion process. Also swirler increases the residence time. At the end swirler increase the combustion efficiency. Basic principle of the swirler is shown in Figure 4.5.

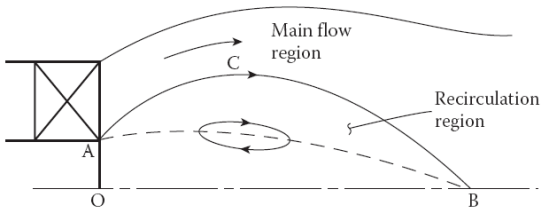

Figure 4.5 Representative Image of Recirculation Region Owing to Swirler [20]

The basic design parameters of the swirler are Swirl Number (SN) and the pressure difference before and after the swirler, which will be investigated in Pressure Loss Module. Swirl number is defined as the ratio of the axial flux of the swirl momentum to the axial flux of the axial momentum times the equivalent nozzle radius. Thus; final form of the swirl number is given by [20],

$$SN = \frac{\int_{R_i}^{R_0} \rho u_z u_\theta 2\pi r^2 dr}{\int_{R_i}^{R_0} \rho \left(u^2{}_z - \frac{u^2{}_\theta}{2} \right) 2\pi R_0 r dr} \qquad 4.15$$

It is known that when SN<0.4 swirl is weak, and SN>0.7 swirl is strong. For a gas turbine type combustor, the SN should be greater than 0.4 for efficient combustion. [30] When SN>0.7, in another words in case of strong swirl, the recirculation flows in the toroidal region becomes very strong and these strong recirculation flow may severely damage the combustion chamber therewithal injector. Because of that, SN should be less than 0.7.

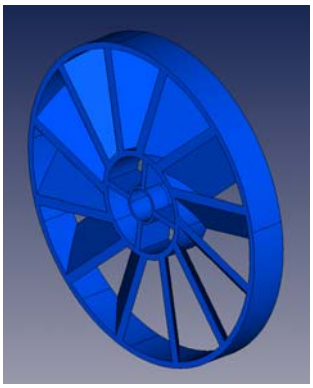

Figure 4.6 CAD Image of the Swirler

Another important design factor in swirler design is the cooling need of the injector where this necessity arose in the combustion chamber analysis. Central part of the swirler was slotted so that injector was cooled by film cooling method. CAD image of this advanced swirler was given in Figure 4.6.

Injector passes through the center of the swirler. Because of this, while generating the swirler geometry; the diameter of the injector tube must be defined. Outer diameter of the swirler is found by considering the equivalence ratio. Flow splitting defines the outer diameter.

Another important design factor of the swirler is the pressure loss of the swirler, ΔP_{sw}. This pressure loss is an important design factor for cooling of the combustion chamber. The cooling air flows out of the combustor to cool the CC liner and penetrates into the CC through the CAH. To prevent the flames to move out the CC, the static pressure in the CC should be less than the static pressure of the cooling air. %3-5 pressure loses in the CC is desirable in gas turbine combustors [20]. In this vitiator design the swirler pressure loss is taken as %3. Equations which used in the design of the swirler were defined in 4.16 to 4.18. The input and output parameters of the swirler design module is given in Table 4.3.

$$\dot{m}_{sw} = \left\{ \frac{2 \times \rho \times \Delta P_{sw}}{K_{sw}((\sec\theta / A_{sw})^2 - 1/ A_L{}^2)} \right\}^{0.5} \tag{4.16}$$

$$A_{sw} = (\pi / 4)(D_{sw}{}^2 - D_{hub}{}^2) - 0.5 \times n \times t(D_{sw} - D_{hub}) \tag{4.17}$$

$$SN = \frac{2}{3} \times \frac{1 - (D_{hub} / D_{sw})^3}{1 - (D_{hub} / D_{sw})^2} \tan\theta \tag{4.18}$$

$\dot{m}_{sw}$	:	Air mass flow rate passing through the swirler	kg/s
ρ	:	Density	kg/m^3
ΔP_{sw}	:	Pressure Loss through the Swirler	Pa
K_{sw}	:	Flat Plate Vane Coefficient	
θ	:	Vane Angle	°
A_L	:	Combustion Chamber Liner Wet Area	m^2
A_{sw}	:	Inlet Area of the Swirler	m^2

D_{sw}	:	Outer Diameter of the Swirler	m
D_{hub}	:	Inner Diameter of the Swirler	m
n	:	Number of Vanes	-
t	:	Vane Thickness	m
SN	:	Swirl Number	-

Table 4.3 Input and Output Parameters of the Swirler Design Module

Input Parameters		**Output Parameters**
Pressure Loss Ratio	:	Outer Diameter of Swirler
CC Pressure	:	CC Inlet Pressure
Air Inlet Temperature	:	Vane angle
Mass Flow Rate of Combustion Air	:	
CC Diameter	:	
Outer Diameter of the Injector	:	
Flat Plate Vane Coefficient	:	
Vane Thickness	:	
Number of Vanes	:	
Swirl Number	:	

4.6 Injector Design Module

Injector module calculates the injection area and total pressure of the methane by given necessary methane mass flow rate and injection velocity. Isentropic relations were used for calculations. Important design equation of the injector is closed form expression for the mass flow through a choked nozzle. Injector which was designed in this thesis adjustable area gaseous injector and the injection area completely depends on the fuel flow characteristics and the CC characteristics. According to known CC pressure, total methane pressure is found by Equation 4.19. After finding the total methane pressure, injection area is found for that operating condition of the combustion chamber by 4.20.

$$\frac{P_0}{P} = \left(1 + \frac{\gamma - 1}{2} M^2\right)^{\gamma/\gamma - 1} \tag{4.19}$$

$$\frac{\dot{m}\sqrt{RT_0}}{A^* P_0} = \sqrt{\gamma \left(\frac{2}{\gamma + 1}\right)^{(\gamma+1)/(\gamma-1)}} \tag{4.20}$$

Input and output parameters of Injector Design Module are given in Table 4.4.

Table 4.4 Input and Output Parameters of the Injector Module

Input Parameters		**Output Parameters**
Necessary Methane Mass Flow Rate	:	Injection Area
Combustion Chamber Pressure	:	Total Pressure of Methane
Injector Exit Mach Number	:	
Methane Inlet Temperature	:	

4.7 Heat Transfer Module

Combustion chamber of the heater must be cooled during the operation. When there is combustion in the liner convective and radiating heat transfer becomes inside the chamber through the liner. Conduction becomes over the liner. Liner cooled with convection by the cooling air. Heat transfer model is given in Figure 4.7 clearly. A resistance model is constructed in the heat transfer module.

Front view of the combustion chamber is given in Figure 4.8. The equations used in the heat transfer calculations were defined from Equations 4.21 to 4.26. Cold side and hot side wall temperatures of the liner are calculated. Cooling air velocity is limited to 50m/s to keep the static pressure above a certain limit and the distance between d_o and D_i is changed for this limitation. CC liner thickness was taken as 1.5mm for this design concordant to literature where Lefebvre states that this value can be taken between 0.75-2mm [20].

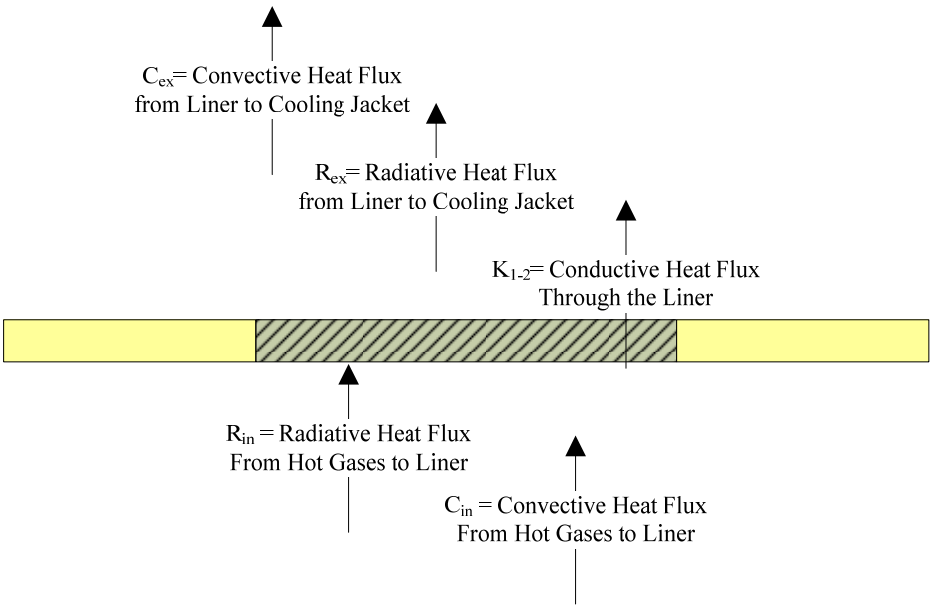

Figure 4.7 Heat Transfer Model

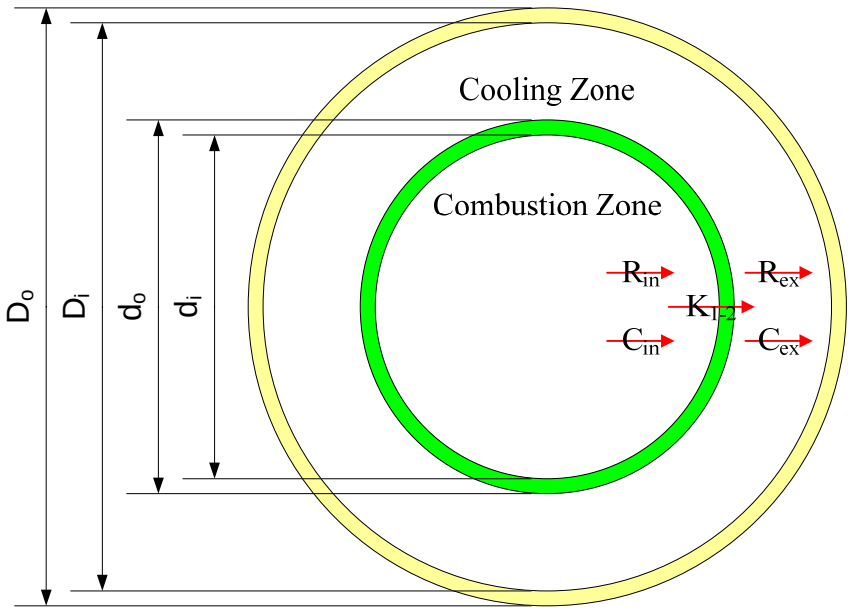

Figure 4.8 Heat Transfer Scheme

Adiabatic flame temperature value is calculated in the chamber according to the ϕ value. Adiabatic flame temperature is allowed to be in the core of the combustion chamber and heat transfer analysis is done to calculate the wall temperature of the CC liner. CC is so found that ϕ value is 0.6 globally without considering the

cooling air. Bu there is some regions where ϕ values are 1 locally. In these regions flame temperatures are higher. Because of this reason flame temperature for $\phi = 0.6$, is multiplied by a safety factor to get more realistic wall temperature values after the heat transfer calculations. Heat transfer calculations are based on the model given in Figure 4.7.

$$R_{in} = 0.5 \times \sigma \times (1 + e_w) \times e_g \times (T_c^{1.5})^{0.5} \times (T_g^{2.5} - T_w 1^{2.5}) \quad 4.21$$

$$R_{ex} = \sigma \times ((e_w \times e_c)/(e_c + e_w \times (1 - e_c) \times \frac{d_o}{D_i})) \times (Tw2^4 - T3^4) \quad 4.22$$

$$C_{in} = 0.0017 \times (k_g / d_i^{0.2}) \times (m_c / (A_l \times \mu_{ug}))^{0.8} \times (T_g - T_{w1}) \quad 4.23$$

$$C_{ex} = 0.020 \times (\frac{k_a}{(D_i - d_o)^{0.2}} \times (\dot{m}_{an} / (A_{an} \times \mu_{ua}))^{0.8} \times (T_{w1} - T_3) \quad 4.24$$

$$K_{1-2} = (k_w / t) \times (T_{w1} - T_{w2}) \quad 4.25$$

$$R_{in} + C_{in} = R_{ex} + C_{ex} = K_{1-2} \quad 4.26$$

σ	:	Stefan-Boltzman Constant	$W/(m^2K^2)$
e_w	:	Emissivity of the Liner	
e_g	:	Emissivity of the Combustion Products	
e_c	:	Emissivity of the Casing	
T_g	:	Temperature of the Products	K
T_{w1}	:	Inner Wall Temperature	K
T_{w2}	:	Outer Wall Temperature	K
T_3	:	Ambient Air Temperature	K
$\dot{m}_{an}$	:	Mass Flow Rate of the Cooling Air	kg/s
μ_{ug}	:	Viscosity of the Cooling Air	kg/(ms)
$\dot{m}_c$	:	Mass Flow rate of Combustion Air	kg/s

μ_{ug}	:	Viscosity of the Combustion Air	kg/(ms)
k_a	:	Conductivity of Cooling Air	W/(mK)
k_g	:	Conductivity of Combustion Air	W/(mK)
k_w	:	Conductivity of the Liner	W/(mK)
A_{an}	:	Cross Section Area of Cooling Air Flow Passage	m^2
A_l	:	Cross Section Area of Combustion Chamber	m^2
t	:	Wall Thickness of the Liner	mm

4.8 Pressure Loss Module

The main pressure loss mechanisms in the combustion chamber are fluid mechanics and combustion loss. The static pressure of the cooling air must be higher than the pressure of the cooling air. The pressure of the combustion air decreases through the swirler. Cooling air is given to the combustion chamber after cooling the liner. The pressure drop in the constant area duct is calculated with the Fanno flow, where the details can be found in reference [22]. This calculation is done to check if the pressure loss of the inner liner is greater than the pressure of the cooling air loss. Otherwise hot products can come out through the CAH's and this can damage the combustion chamber. A Pressure Loss Module was generated to calculate the pressure loss. The input and output parameters of the Pressure Loss Module are given in Table 4.5. Loss of the swirler is taken into account %3 in the Pressure Loss Module.

Table 4.5 Input and Out Parameters of the Pressure Loss Module

Input Parameters		**Output Parameters**
Mass Flow Rate of Cooling Air	:	Pressure Loss of the Constant Area Duct
Temperature of the Cold Air	:	
Combustion Chamber Inlet pressure	:	
Combustion Chamber Length	:	
Combustion Chamber Diameter	:	
Diameter of the Swirler	:	

4.9 Design of the Vitiator

The operating conditions of the heater are given in Table 4.6 and the basic design criterion is given in Table 4.7. The design of the vitiator is completed and the basic geometrical values of the combustion chamber are given in Table 4.8. All the pressure, temperature, mass, length, angle and time values were normalized in this thesis.

Table 4.6 Operation Conditions of the Vitiator

Definition		Normalized Values
Air Inlet Temperature	:	0.50
Methane Inlet Temperature	:	0.50
Oxygen Inlet Temperature	:	0.50
Exit Temperature	:	1.64
Total Mass Flow Rate	:	1.00
Exit Pressure of Vitiator	:	1.68

Table 4.7 CCDC Basic Design Criteria

Definition		Value	Unit
CLP	:	1	-
Global ϕ in the CC	:	0.6	-
Mach number in the CC	:	0.02	-
Swirler Total Pressure Loss	:	%3	-
Swirl number	:	0.6	-
Velocity of the Cooling Air	:	50	m/s
Number of cooling holes on the CC	:	40	-
Injector Exit Mach Number	:	1.0	-

Table 4.8 Basic Geometrical Values of the Combustion Chamber

Definition		Normalized Values
CC Length	:	3.67
CC Diameter	:	1
Diameter of Cooling Holes	:	0.06
CC Divergence Angle	:	2.05

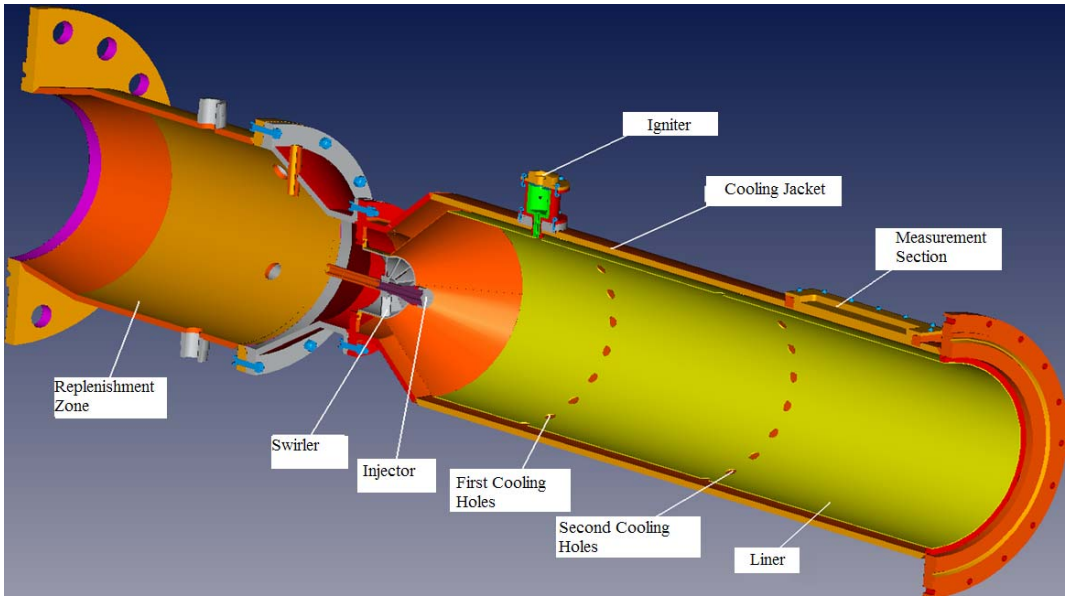

Figure 4.9 General View of the Vitiator

CHAPTER 5

REACTING FLOW CFD ANALYSIS

Initial CFD analysis was performed to determine the effect of the design parameters on combustion. The analysis method, models used in the analysis and the assumptions for the analysis were explained in this part.

Important parameters effecting combustion are given as follows:

- Fuel Injector Position (FIP)
- Combustion Chamber Divergence Angle (CCDA)
- Swirler Vane Angle (SVA)

Fuel injector position is important for several reasons. FIP directly affects mixing characteristics thereby combustion efficiency. If the injector is located close to the swirler, combustor or swirler may damage. Because of the strong recirculation zone, fuel can have high concentration close to the swirler and there may be high temperature close to the combustion chamber, swirler and injector.

Divergence angle is important by virtue of interaction with swirler. When CCDA is high enough, the desired toroidal flow cannot be get; the combustion is completed close to end of the combustion chamber or not. Accordingly, appropriate divergence angle should be decided.

Swirler creates a toroidal flow and a recirculation zone is generated in this toroidal flow. This recirculation zone provides good mixing. If the intensity of this

swirling is high, combustion takes place close the swirler and around the injector. If the intensity is low, then there can't be enough mixing; it means inefficient combustion. Therefore swirl number should be kept in a certain interval. Consequently FIP, CCDA and SVA should be chosen for the final design of the vitiator. These parameters are shown in Figure 5.1 on the computational domain.

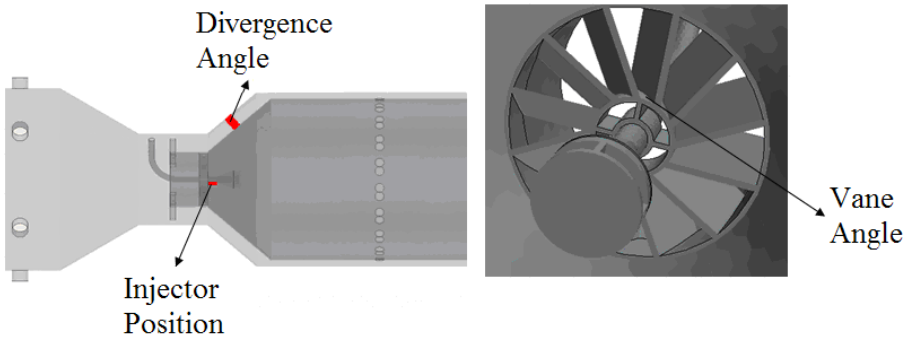

Figure 5.1 FIP, CCDA and SVA Parameters

There is a gap between fuel injector and Swirler as it is shown in Figure 5.1. Some part of the combustion air pass through this gap. It is mainly for cooling of injector. Line probes were defined after a certain distance of swirler to read the values of the desired parameters. Resolution for the probes is 20; it means 20 points were assigned for each probe. These line probes were shown in Figure 5.2.

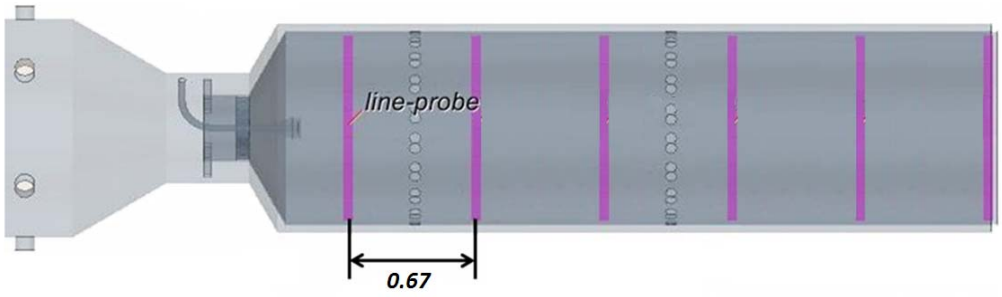

Figure 5.2 Line Probes

An analysis plane was constructed to monitor the results. This plane is shown in Figure 5.3 and temperature, concentration, pressure, i.e., can be read on this plane.

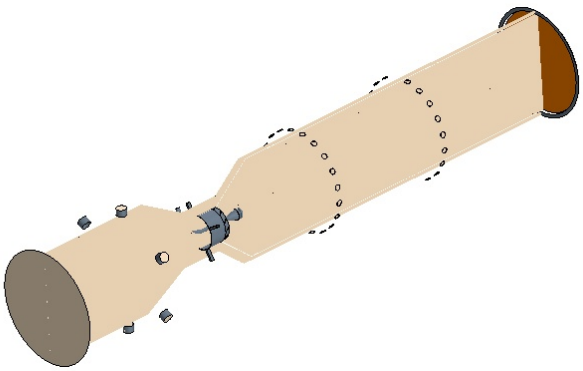

Figure 5.3 Monitoring Plane

5.1 Initial CFD Analysis

11 different geometrical configurations were constructed and reactive CFD analyses were done. Configurations and variables are given in Table 5.1. Hexagonal mesh was constructed and the number of the meshes is also given.

Table 5.1 Geometrical Configurations and Mesh Size (Normalized)

Configuration	SVA[1]	FIP[1]	CCDA[1]	Mesh Number
1	1.5	0.12	2	764046
2	1.5	0.05	3	754600
3	1.5	0.05	2	747482
4	1.75	0.12	3	781214
5	1.75	0.12	2	838344
6	1.75	0.05	3	753870
7	1.75	0.05	2	755275
8	2.05	0.12	3	799272
9	2.05	0.12	2	750973
10	2.05	0.05	3	755912
11	2.05	0.05	2	734001

[1] All data were normalized except mesh number

5.2 Models Used for CFD Analysis and Assumptions

Combustion chamber design includes complex physical and chemical problems. To solve these problems, 3 dimensional analyses should be done, turbulence must be taken into account and correct combustion model must be used.

Grid number of the computational domain is an important factor for the analysis. It is unavoidable to get wrong results to numerical discritization for a bad structured mesh. Also turbulence model has big importance for the discritization and circulation estimation. Correct turbulence model and model coefficients should be chosen for the analysis. Eddy Break Up combustion model and standard $k-\varepsilon$ turbulence model were used for the analysis. These models were preferred because of their middling results. The important parameter in $k-\varepsilon$ turbulence model is turbulence intensity. For high turbulence case, the turbulence intensity becomes typically between 5-20% [34],[35]. In our case intensity value was considered as 10%.

For the combustion analysis it is assumed that the combustion completed in 3 steps. Important reactions are reduced between Equations 6.1 to 6.3. CO, O and H steps of high temperature methane oxidation is important and these steps are reformed to combine a complete oxidation reaction. These reactions were introduced to CFD code and 3-Step Eddy Break Up combustion analysis were performed.

$$CH_4 + \frac{1}{2}(O_2 + 3{,}76N_2) \rightarrow CO + 2H_2 + 1{,}88N_2 \qquad 6.1$$

$$CO + \frac{1}{2}O_2 \rightarrow CO_2 \qquad 6.2$$

$$H_2 + \frac{1}{2}O_2 \rightarrow H_2O \qquad 6.3$$

5.3 Results of the Initial CFD Analysis

Simulation results are given in Table 5.2. Mesh numbers are given in Table 5.1 and it is clear that the results are not subjected to the mesh numbers.

Temperature distribution of all configurations is given on the same scale and is given in Figure 5.4. Left hand side images in Figure 5.4 are for the CCEA=3. The highest temperature in the combustion chamber for the CCEA=3 geometries becomes at the end of the combustion chamber. For further analysis CCEA=3 geometries were elected. In remaining configurations, it was evaluated that combustion is completed earlier in 9^{th} and 11^{th} configurations. To evaluate 9^{th} and 11^{th} configurations better, the temperature distribution to the adjacent grid points of the injector and CO mass fraction distributions were observed.

It is observed that, the temperature values to the adjacent grid points of the injector for 9^{th} configuration is smaller than 11^{th} configuration. There are also some hot points on the 9^{th} configuration but it is evaluated that configuration 9 is more safe than 11^{th} configuration.

CO distribution can be described as the foot steps of combustion. The places where CO exists can be said that combustion exists. CO distribution is given in Figure 5.6 and according to this figure combustion is completed earlier for the 9^{th} configuration. 9^{th} configuration was chosen for the detailed analysis and 9^{th} configuration will be called as chosen configuration in the remaining part of the thesis.

Table 5.2 Product Characteristics

Config.	Mass Fractions of the Main Products (%)									
	CH_4	CO	H_2	CO_2	H_2O	N_2	O_2	O_2 (mol)	T_e[2]	P_e[2]
1	0.00	0.02	0.00	3.24	2.69	70.57	23.43	21.10	1.55	1.76
2	0.00	0.02	0.00	3.29	2.69	70.58	23.42	21.09	1.56	1.77
3	0.00	0.03	0.01	3.26	2.66	70.57	23.46	21.13	1.54	1.76
4	0.00	0.04	0.01	3.25	2.65	70.57	23.47	21.14	1.54	1.78
5	0.00	0.00	0.00	3.32	2.72	70.57	23.37	21.04	1.58	1.77
6	0.00	0.03	0.00	3.27	2.67	70.58	23.44	21.11	1.55	1.78
7	0.00	0.01	0.00	3.32	2.71	70.57	23.39	21.05	1.58	1.77
8	0.00	0.01	0.00	3.31	2.71	70.57	23.39	21.06	1.58	1.79
9	0.00	0.00	0.00	3.31	2.71	70.58	23.40	21.06	1.59	1.78
10	0.00	0.02	0.00	3.29	2.69	70.58	23.42	21.08	1.57	1.79
11	0.00	0.00	0.00	3.31	2.71	70.58	23.40	21.06	1.59	1.78

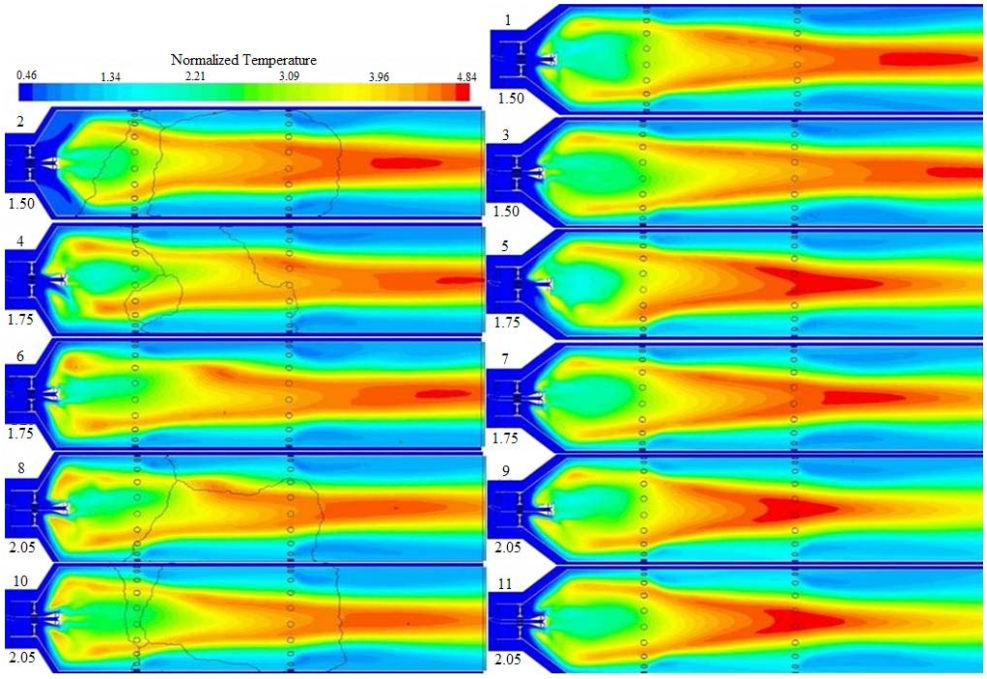

Figure 5.4 Total Temperature Distribution on Monitoring Plane

[2] Temperature and pressure values were normalized

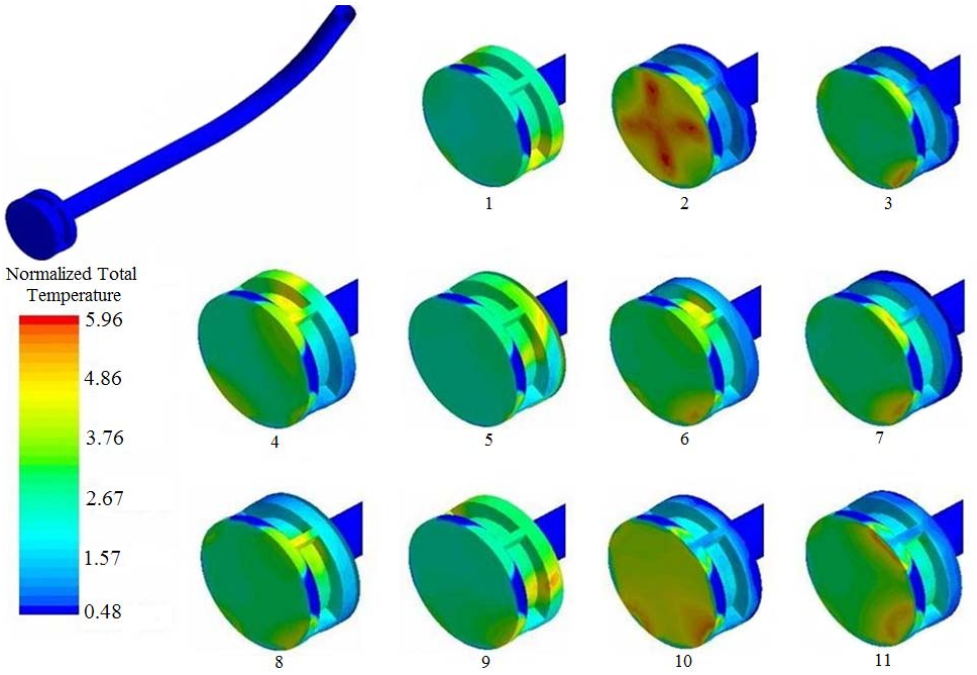

Figure 5.5 Temperature Distribution on the Grid Points Adjacent to the Injector Wall

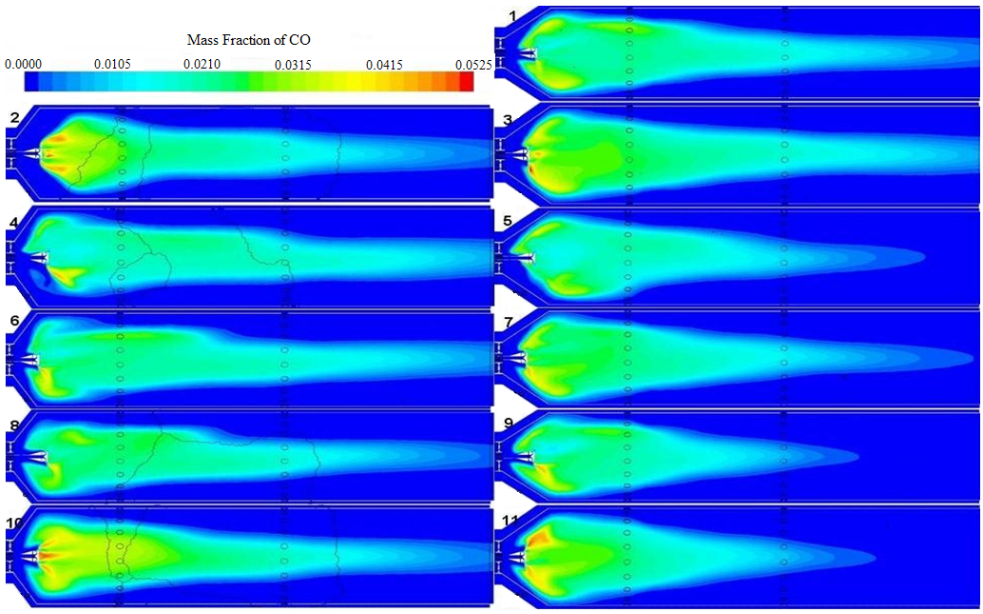

Figure 5.6 CO Mass Fraction Distribution on Monitoring Plane

5.4 Detailed Reacting Flow CFD Analysis of the Chosen Configuration

Combustion analyses have been done by using Standard $k-\varepsilon$ and SST $k-\omega$ turbulence models and the results were compared. The parameters without turbulence were kept constant. Therefore, the differences are originated from turbulence models.

SST $k-\omega$ model works as a hybrid model. In Shear Stress Transport (SST) $k-\omega$ model approach, standard $k-\omega$ model is used close to the wall and $k-\varepsilon$ is used in the chamber. Combustion completes slowly with the SST $k-\omega$ turbulence model. Temperature distribution is shown in Figure 5.7. Mass fraction of CO and global mass fraction of H and C included molecules are shown in Figure 5.8 and Figure 5.9 respectively.

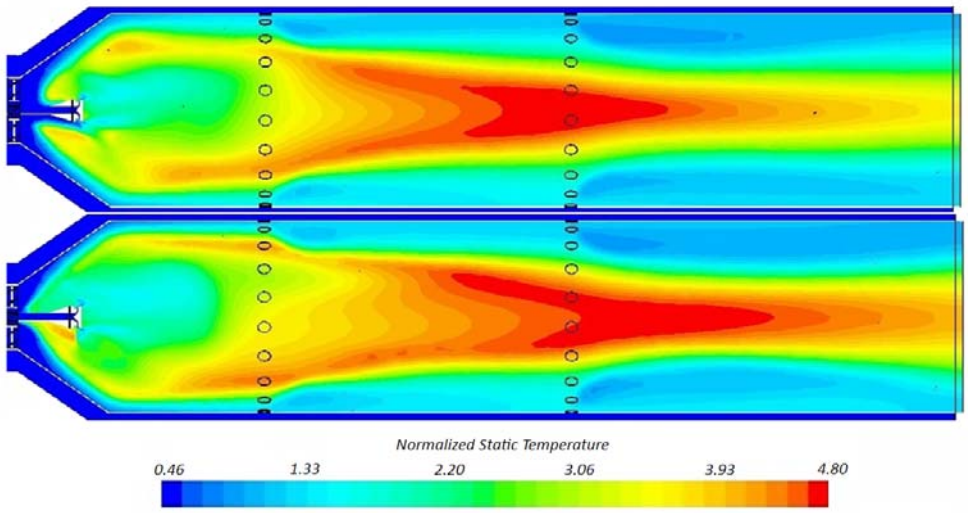

Figure 5.7 Static Temperature Distribution for Standart $k-\varepsilon$ ve SST $k-\omega$ Turbulence Models

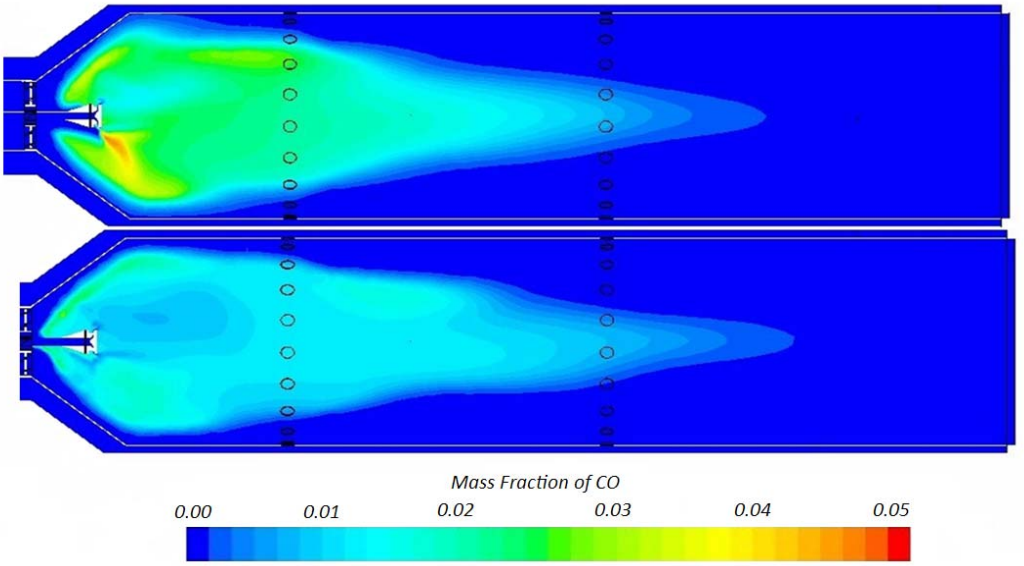

Figure 5.8 CO Mass Fraction Distribution for Std. $k-\varepsilon$ ve SST $k-\omega$ Turbulence Models of Chosen Configuration

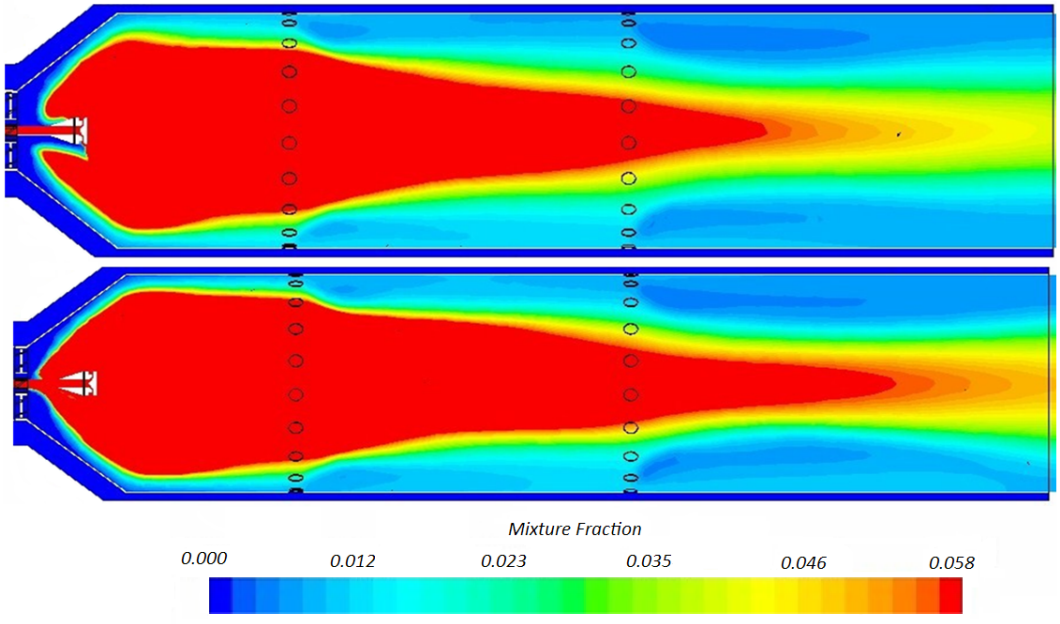

Figure 5.9 Mixture Fraction Distribution for Std. $k-\varepsilon$ ve SST $k-\omega$ Turbulence Models of Chosen Configuration

Mixture Fraction changes with the oxygen mass fraction. If the entering oxygen quantity increases in the combustion chamber, the mass ratio of H and C decreases. In another words the higher mixture fractions, the less air mass fraction of air.

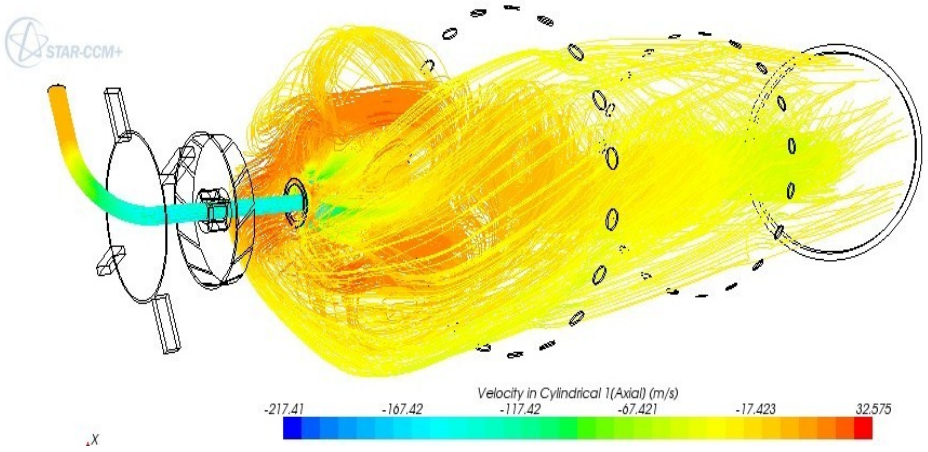

Figure 5.10 Streamlines of Methane for Chosen Configuration

Methane streamlines is shown in Figure 5.10 for the $k-\varepsilon$ turbulence model. The toroidal flow region can be seen easily from these streamlines.

Probe points were assigned to calculate the axial temperature distribution in the vitiator as shown in Figure 5.11. As a result axial temperature distribution is obtained as shown in Figure 5.12. The temperature drastically drops to the cooling points. The average exit temperature becomes nearly constant at the end of the combustion chamber. Also theoretical adiabatic temperature and average total exit temperature are also compared at the exit. It is expected that adiabatic flame temperature and average total exit temperature are the same. But average total exit temperature is slightly less than adiabatic flame temperature.

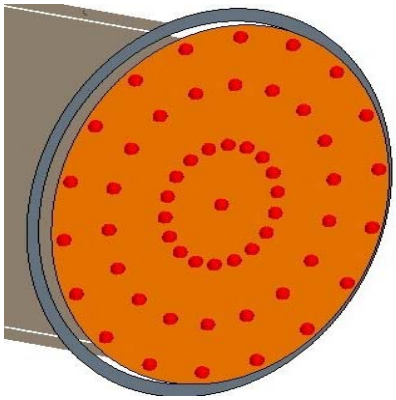

Figure 5.11 Probe Points for Average Radial Temperature Distribution in the Heater

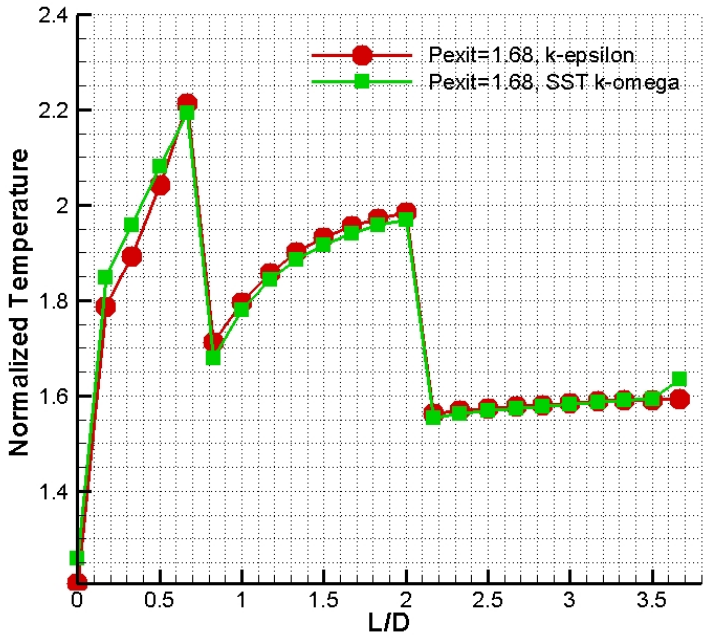

Figure 5.12 Normalized Average Axial Temperautre Distribution for Standard $k-\varepsilon$ and SST $k-\omega$ Turbulence Models

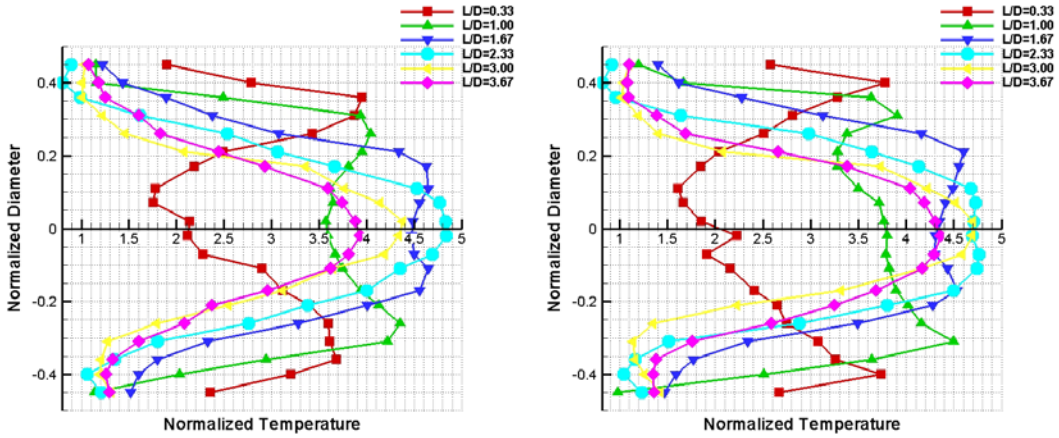

Figure 5.13 Radial Temperautre Distribution for Standard $k-\varepsilon$ ve SST $k-\omega$ Turbulence Models

Second order solutions of the radial temperature distribution are given in Figure 5.13. Temperature values are lower close to wall because of the film cooling. Asymmetrical temperature distribution in the primary zone becomes symmetrical at the end of the combustion chamber.

5.5 Off-Design Analysis for the Chosen Configuration

Boundary conditions for the off-design operating conditions are given in Table 5.3.

Table 5.3 Boundary Conditions of Chosen Configuration for Off-Design Analysis

Total Exit Pressure[3]	**Inlet Air Total Temperature**[3]	**Mass Flow Rate of CH_4**[3]	**Mss Flow Rate of O_2**[3]	**Mass Flow Rate of Air**[3]
1.17	0.50	0.01	0.03	0.53
1.45	0.50	0.01	0.04	0.64

Temperature distribution is given in Figure 5.14. Combustion is completed in the primary zone for all configurations. When the pressure decreased from 1.68 to

[3] All data were normalized

1.17 and 1.45 (normalized pressures), mass flow rates decrease as a result; combustion starts earlier. The residence time increases according as decreasing combustion chamber pressure.

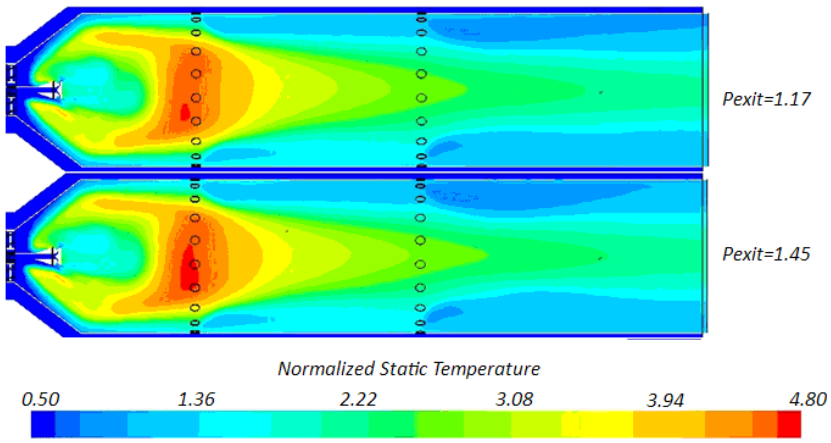

Figure 5.14 Static Temperature Distribution for Off-Design Conditions

The temperature distribution on the injector is given in Figure 5.15. It is understood that, the temperature is close to 3.80 (normalized) and this temperature is considered safe for the injector material.

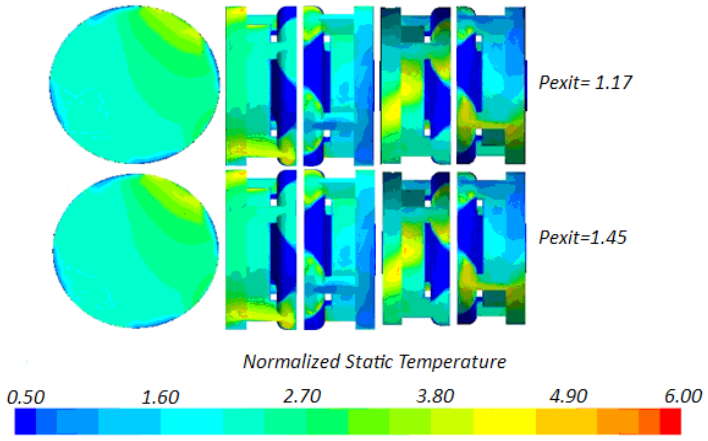

Figure 5.15 Static Temperature Distribution on Injector for Off-Design Conditions

CO distribution is given in Figure 5.16. High concentration of CO near the injector means that combustion starts in this region after mixing of air and methane.

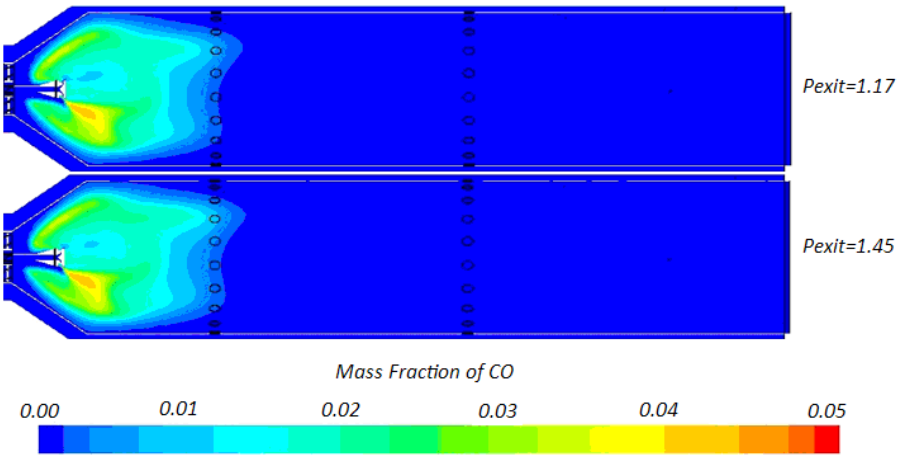

Figure 5.16 CO Mass Fraction for Off-Design Conditions

Axial temperature distribution is given in Figure 5.17. Rapid temperature falls, indicates the cooling holes. Temperature fixed at the end of combustion chamber. Exit temperature is almost the same with the theoretical adiabatic flame temperature. Radial temperature distribution is given in Figure 5.18. Temperature alterations are as expectedly. When the pressure decreased, asymmetry of the distribution decreases.

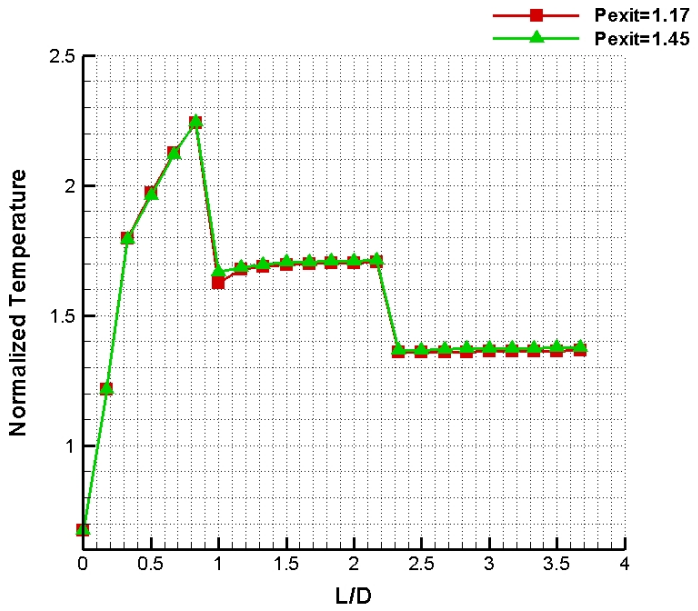

Figure 5.17 Axial Temperature Distribution for Off-Design Conditions

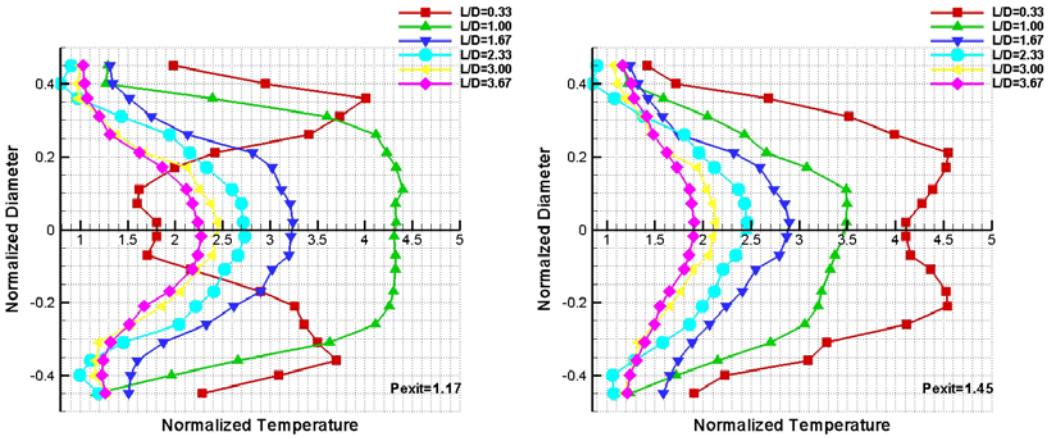

Figure 5.18 Radial Temperature Distribution for Off-Design Conditions

5.6 Investigation of Pressure Loss, Residence Time

Residence time and pressure drop of the combustion chamber was observed for every configuration and the results are given in Table 5.4.

Residence time must be greater than 10ms for efficient combustion. When the results analyzed, it is concluded that the residence time is enough for the completion of the combustion.

Maximum Pressure Drop of the combustion chamber, ΔPcc, is desired %5. When the results were compared, it is clearly seen that the ΔPcc is in the range of %2-3. These values are also consistent with the swirler pressure drop. It is also seen that, pressure drop decreases with the decreasing pressure. Pressure loss, $\Delta Psch$, sourced by the cooling holes defined as follows:

$$\Delta Psch = \frac{\Delta P}{P_{03}} \qquad 6.4$$

This pressure loss is proportional with the penetrating coolant air. This value should be under %5. Highest pressure loss is found as %4.75. The results are found quite successful. $\Delta Psch$ increases with increasing combustion chamber

pressure. Also cooling air comparison is given in Table 5.5. It is clearly seen that primary and secondary cooling air coming into the combustion chamber almost the same.

Table 5.4 Pressure Loss, Residence Time and Loading Factor Results

Chosen Configuration	τ **(ms)**	ΔPcc **(%)**	$\Delta Psch$ **(%)**
$k-\varepsilon$ Turb. Model (P_{exit}=8.4Bar)	39.5	2.96	4.66
SST $k-\omega$ Turb. Model (P_{exit}=8.4Bar)	39.5	2.83	4.75
P_{exit}=5.87Bar	55.0	1.88	3.10
P_{exit}=7.23Bar	56.2	1.90	3.08

Table 5.5 Mass Flow Rate Distribution After Splitting for Different Conditions

Chosen Configuration	**Total Cooling Air[4]**	**Primary Cooling Air[4]**	**Secondary Cooling Air[4]**	**Combustion Air[4]**	**Total Mass Flow Rate[4]**
$k-\varepsilon$ (P_{exit}=8.4Bar)	0.57	0.30	0.26	0.42	0.99
SST $k-\omega$ (P_{exit}=8.4Bar)	0.56	0.30	0.26	0.43	0.99
(P_{exit}=5.87Bar)	0.32	0.17	0.15	0.25	0.56
(P_{exit}=7.23Bar)	0.38	0.20	0.18	0.29	0.67

5.7 Conjugate Heat Transfer Analysis

Conjugate Heat Transfer (CHT) analyses were performed to calculate combustion chamber wall temperatures. These analyses necessitate high computational power. More simple geometry was generated to make CHT analysis as given in Figure 5.19. Premixing oxygen zone was removed and oxygen inlets were defined as shown in the Figure 5.19. Initial and boundary conditions were given according to the operating conditions which were given in Table 4.6.

[4] All data were normalized

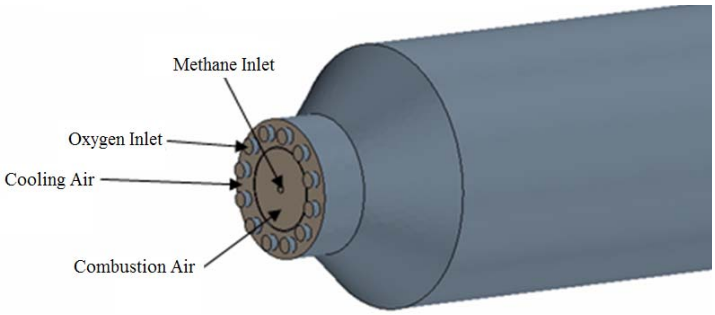

Figure 5.19 CHT Analysis Geometry

Mesh structure for the CHT analysis is shown as in Figure 5.20 and Figure 5.21. The intersection points of the combustion and cooling air volume mesh and liner mesh are the same. Knowledge transfer between volume mesh and liner mesh becomes more efficient.

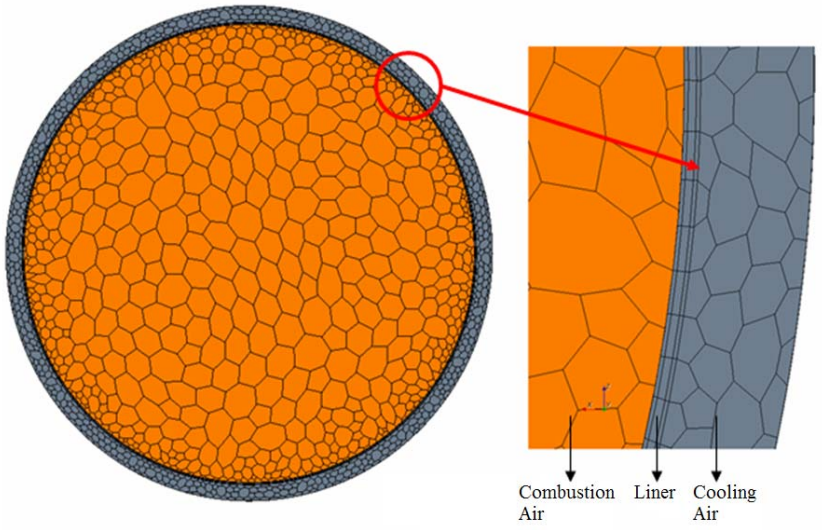

Figure 5.20 Cross Section View of CHT Mesh Structure

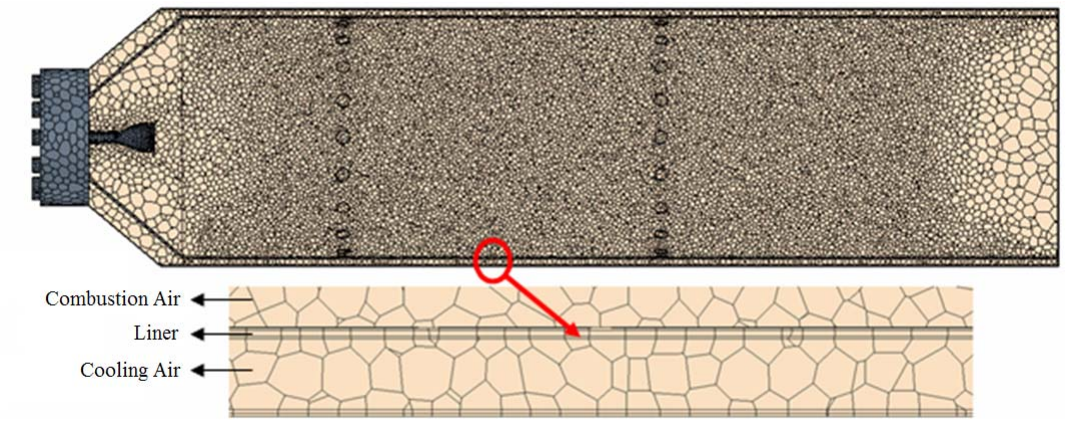

Figure 5.21 Side View of CHT Mesh Structure

Conduction, convection and radiation models are additionally used in CHT analysis contrarily to the former analysis. Temperature distribution on the liner is given in Figure 5.22, on the analysis plane in Figure 5.23 and the axial temperature distribution on the liner is shown in Figure 5.24. The liner is cooled very well until cooling channels. There is only insignificant high temperature region can be seen around the first cooling holes. After second cooling holes the cooling air velocity becomes nearly zero, convection affect of air diminishes and this part is not cooled enough. Temperature values reach nearly 1.4 (normalized) on the liner. This temperature values does not reduce the structural resistance of the liner. But possible third row cooling air holes can reduce this temperature value in more elegant levels.

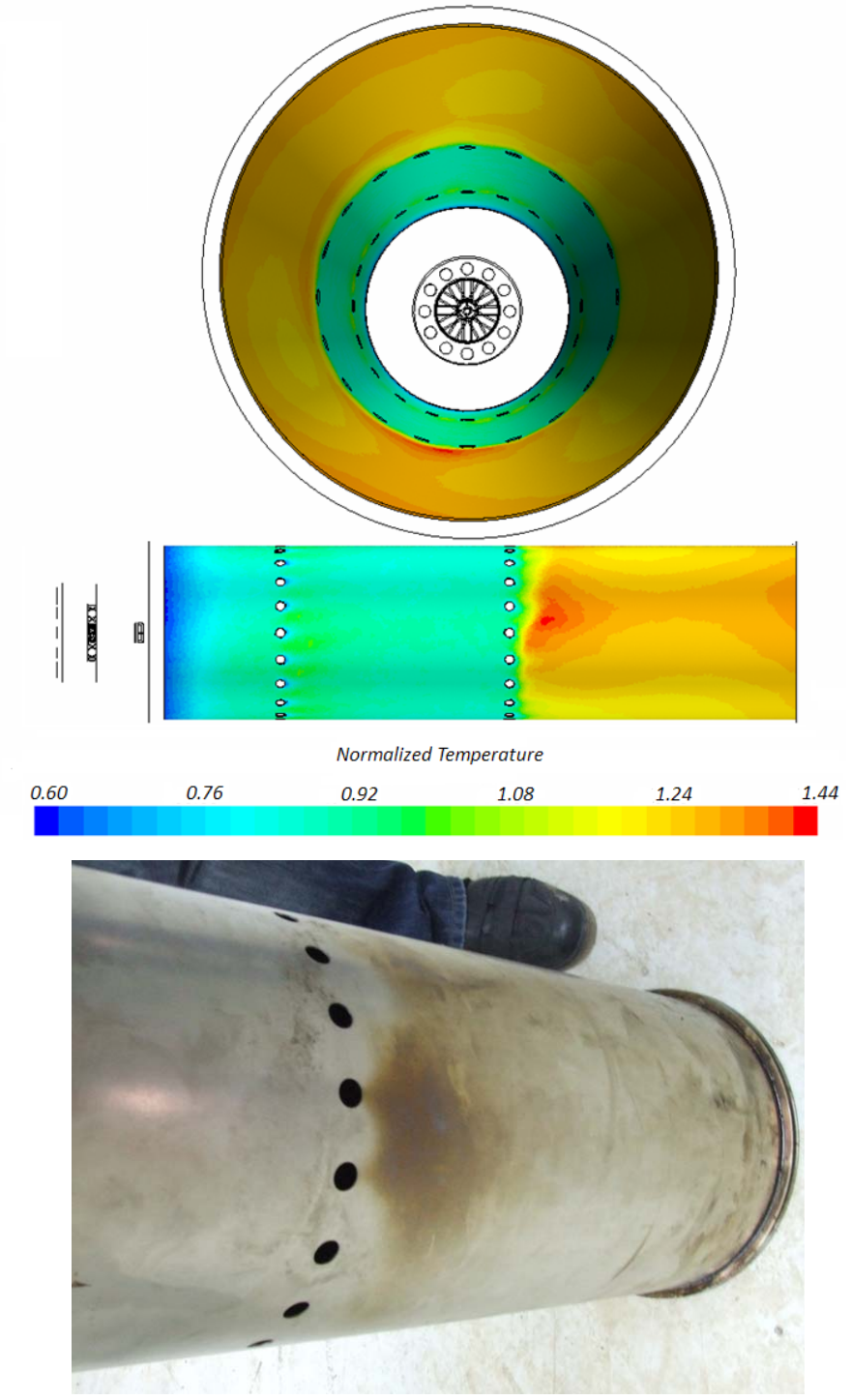

Figure 5.22 Temperature Distribution on the Liner

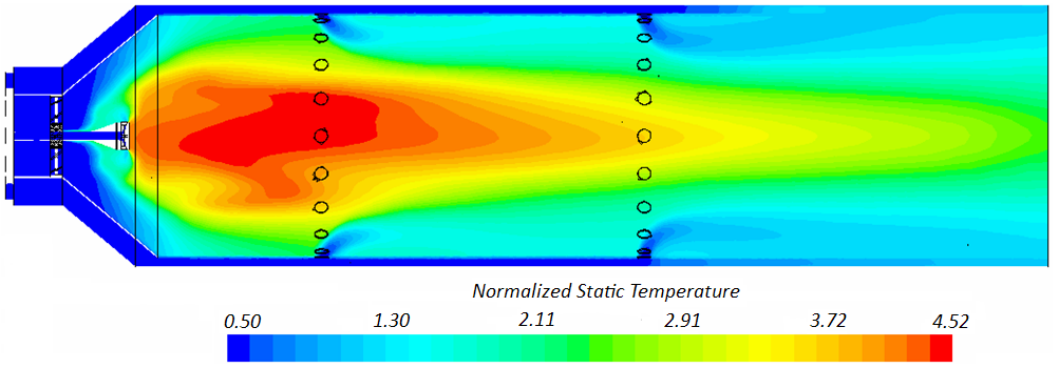

Figure 5.23 Temperature Distribution on the Analysis Plane for CHT

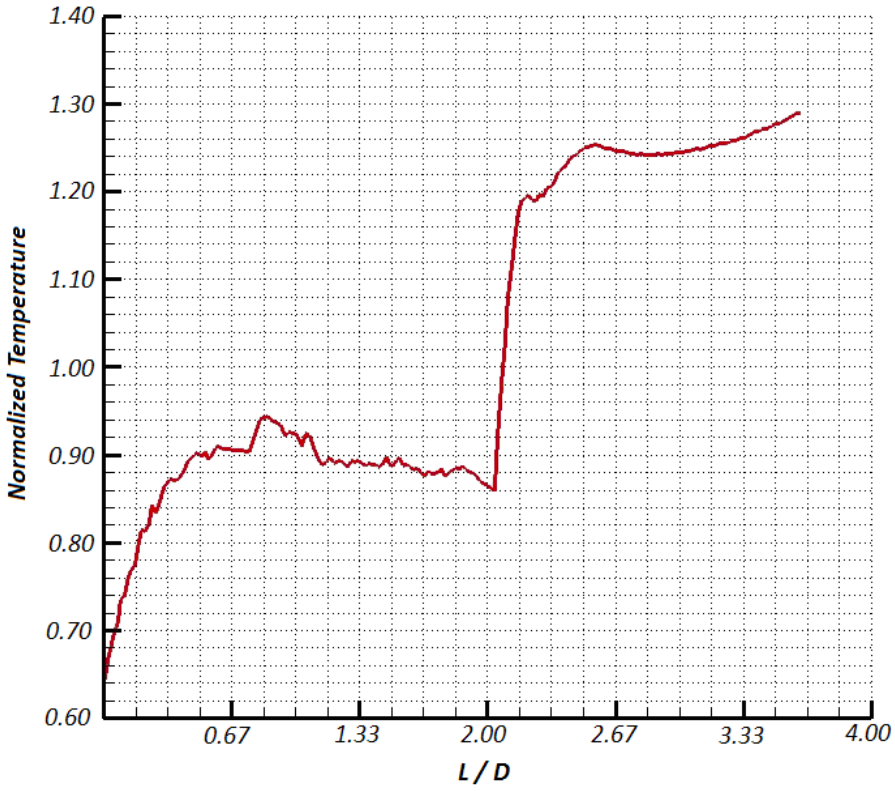

Figure 5.24 Axial Temperature Distribution on the Liner

CHAPTER 6

EXPERIMENTS, RESULTS AND DISCUSSION

6.1 Introduction to Test Setup

The designed vitiator was manufactured and tested with a prototype heater feeding system as shown in Figure 6.1. Performance criteria were considered as the average total exit temperature, product composition. Only exit temperatures were measured because emission measurement system was not ready.

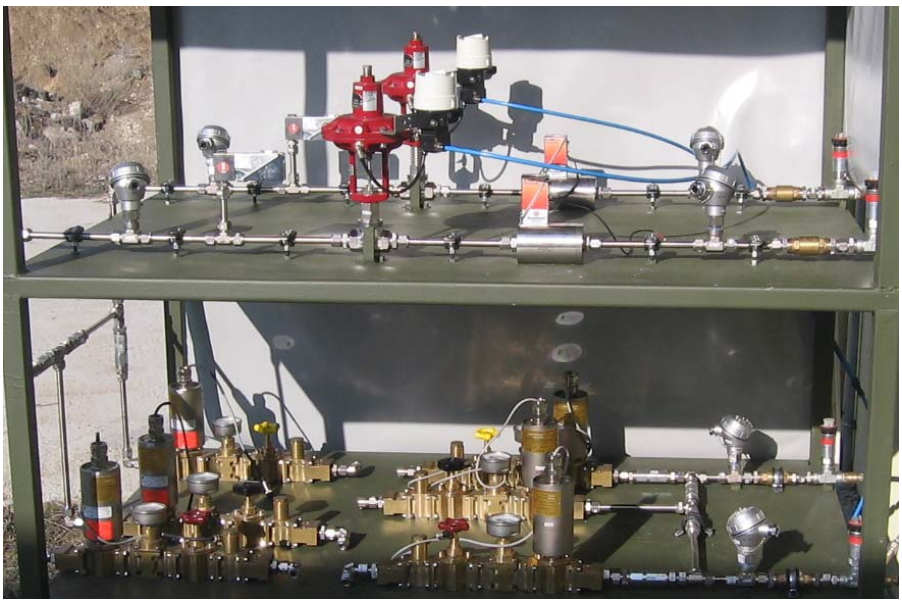

Figure 6.1 Prototype Heater Feeding System

The control program was developed by Labview and National Instruments Compaq Data Acquisition Unit used to control system. The user interface and the generic architecture of the control module are given in Figure 6.2 and Figure 6.3 respectively.

Figure 6.2 Control System User Interface Prepared by Labview

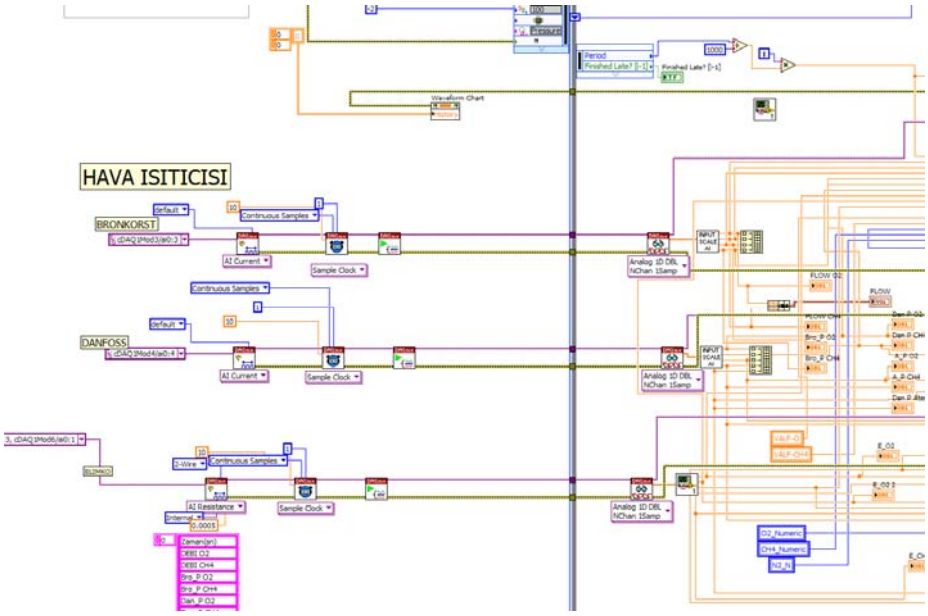

Figure 6.3 Control Module Architecture Prepared by Labview

Combustion started by a pilot flame igniter. A firing view during the characterization test of the pilot igniter is given in Figure 6.4. Igniter is started with a classical automobile spark plug. Pure Methane and Oxygen is used as fuel and oxidizer. Igniter can work 6 (normalized) time units without any failure. It is specially insulated to resist to the high thermal loads. Flame temperature is close to

2.55 normalized temperatures after 0.17 units from the exit of the igniter. This value is quite enough to ignite the vitiator. 0.4 time unit ignition is enough to start the combustion. During the ignition Methane and Oxygen pressure values were kept 3 and 1.8 normalized pressures respectively. Nothing happened to the spark plugs for 0.4 time unit but when the ignition times exceeded 2.5 time units the spark plugs are completely damaged.

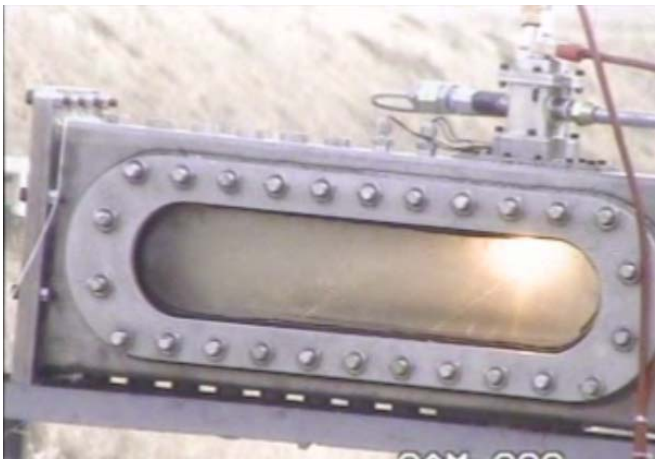

Figure 6.4 Firing of the Pilot Flame Igniter During the Characterization Tests

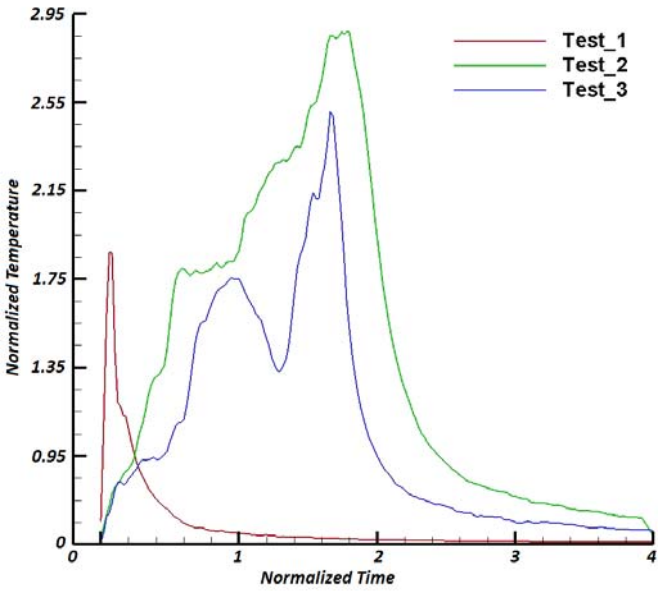

Figure 6.5 Ignitor Flame Temperatures Test 5cm Away the Igniter Exit

6.2 Results of the Tests

The aim of the tests can be said as follows and the test view can be seen in Figure 6.6. Also heater test conditions are given in Table 6.1.

- To start the igniter under real operating conditions
- To start the combustion and continue without blow out.
- To check the repeatability of the tests
- To show if the CC structurally and thermally executes its function

Figure 6.6 Video Camera View During the Heater Tests

Table 6.1 Heater Test Conditions

Test Name	Test Pressure[5]	Air Mass Flow Rate[5]	Heater Exit Temperature[5]	Test Duration[5]
Heater Test-1	1.74	0.12	1.10	4.80
Heater Test-2	0.74	0.23	1.40	17.40
Heater Test-3	0.76	0.25	1.40	37.00

[5] All data were normalized

In the first test, the pressure of the air was close to the analysis cases but because of the low feeding capacity there wouldn't be given enough methane to increase temperature of the full capacity air. Hence 0.12 unit air was given to the combustion chamber and the average total temperature of the air kept 1.1 normalized temperature. Duration of the first test was kept 4.80 times unit. Combustion chamber was investigated and any damages were found. Air mass flow rate and temperature was increased, the pressure was decreased in the second test. Test duration was elevated to the 17.40 time units. For the high velocities in the combustion chamber operability of the combustor was shown. The 2nd test was repeated for the same conditions and repeatability was proved. Duration of the 3rd test was 37 time units and this value is more than the target capacity of the heater. A view during the test can be seen in Figure 6.7. During the 2nd and 3rd tests, exit temperature data was taken by meticulously protected 3 thermocouples and thermal cameras and the results were given in Figure 6.8. It is thought that combustion completed in the combustion chamber because of there is not flame out of the combustion chamber. Detailed measurement of concentrations will show the real emission results and will give opportunity to us evaluate the combustion efficiency. The tests will be repeated after completion of the target capacity heater feeding system.

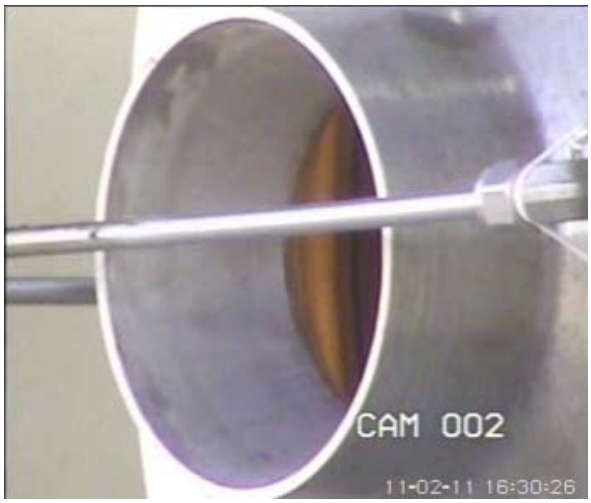

Figure 6.7 During the 3rd Heater Test

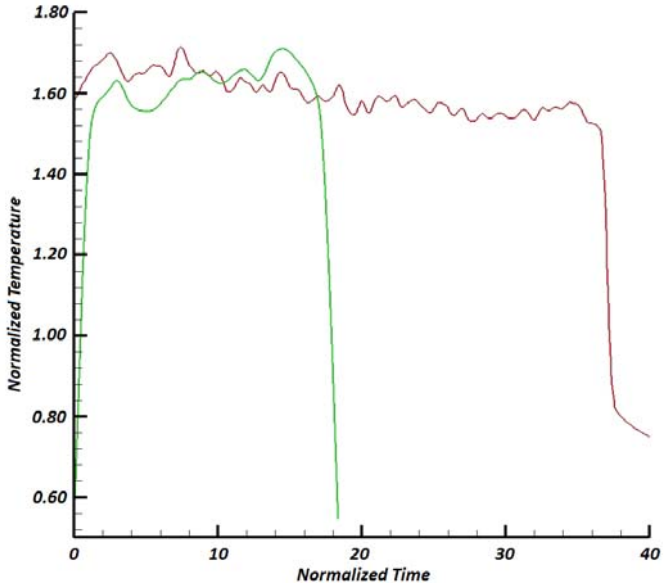

Figure 6.8 Temperature Measurements of the 2nd and 3rd Tests

When the injector investigated after the 2nd and 3rd tests, a small soot region can be seen in front of the swirler. Any deformation became on the injector or swirler at the end of the tests. Injector mounted on the swirler after the tests is shown in Figure 6.9. There was not any deformation on the combustion chamber but only a small region of tempering on the wall close to the second cooling holes which is very similar to the CHT analysis. This color alteration corresponds to nearly 1.4 normalized temperatures. It was verified that heater worked successfully close to the temperature design limits.

Figure 6.9 Injector with Swirler and Liner After the 3rd Test

CHAPTER 7

CONCLUSION AND RECOMMENDATIONS

A combustion chamber design code was constituted and a combustion type air vitiator was designed in the content of thesis. Reactive CFD analyses were performed after defining design limits.

Eddy Break-up combustion model and standard k-ε turbulent models were used to evaluate possible design alternatives. Analyses were performed time independently. Computational capacity was taken into account and maximum hexagonal cell number kept 800000 for the solution domain. Best configuration was decided and more detailed CFD analysis was performed for better characterization of the vitiator.

Standard $k-\varepsilon$ and SST $k-\omega$ models were preferred for the detailed CFD analysis of chosen configuration. It was found that the analysis results are close to the analytical results and there is slight difference between standard $k-\varepsilon$ and SST $k-\omega$ models. Off design analysis were performed after the detailed analysis.

Pressure levels were reduced for off design analysis. Even the pressure levels were reduced and the flow characteristics were changed, combustion was completed earlier. This unexpected result gives possibility use the vitiator in low pressures and mass flow rates.

In all configuration asymmetrical temperature distributions are observed. The possible guilty are toroidal flow in the chamber and the wake of the injector tube behind the swirler.

Residence time, and pressure losses were investigated and the results were found quite reasonable. There is enough time for completion of reactions in the chamber. Pressure losses are as wanted and very close to the analytical results.

CHT analysis was performed after CFD analysis, and it was found that the maximum temperature on the combustion chamber did not exceed the structural limits.

First operational tests of the vitiator were performed. No anomaly was observed during the tests. Combustion seems to complete into the combustion chamber according to video camera results. Average exit temperatures were measured and it was found that the results are close to the analytical results. A hot region was observed which is concordant with the CHT analysis. Main reason of this hot region is toroidal flow in the combustion chamber.

First successful design and test of the vitiator was performed for a high speed wind tunnel at the end of this thesis.

As future works detailed analysis may be done for real boundary conditions after the final tests and CFD the results may be compared by the real test data.

Real temperatures on the combustion chamber line may be found by thermocouples or thermal paint and the results may be compared with CHT analysis results.

REFERENCES

[1] Gruber M., Donbar J., Jackson K., Marthur T., Baurle R., Eklund D., Smith C.: "*Newly Developed Direct Connect High Enthalpy Supersonic Combustion Research Facility*", Journal of Propulsion and Power, Vol. 17, No. 6, 2001

[2] Anderson T., Lucht R., Meyer T., Mathur T., Gruber M., Carter C.; "*Measurements Of NO And OH Concentrations In Vitiated Air Using Diode Laser Based Ultraviolet Absorption Sensors*", AIAA 2007-467, Propulsion Sciences Branch Aerospace Propulsion Division, 2006

[3] Streby G.D., Mathur T., Chen T.H., Akens W., "*Advanced Airbreathing Hydrocarbon-Fueled Aero-Engine Concepts*", AFRL-PR-WP-TR-1999-2038, Ohio, 1999

[4] Netzer D., Brophy C., Conner H., Scruton Z., Robınson J., Hofstedt T., Johnson R., "*The Rocket Propulsion and Combustion Laboratory*", Naval Postgraduate School, M. Sc Thesis, 1999

[5] Netzer D. W., Sınıbaldı J., Brophy C., "*Detonation of a JP-10/Aerosol for Pulse Detonation Applications*", Naval Postgraduate School, M. Sc Thesis, 2000

[6] AGARD-AR-323: "*Experimental and Analytical Methods for the Determination of Connected-Pipe Ramjet and Ducted Rocket Internal Performance*", July, 1994

[7] Puster L. Rıchard, Rock K., Diskin G., "*Direct-Connect Supersonic Combustion Test Facility*", NASA Langley Research Center, Virgina

[8] Huebner, L. D., Rock, K. E., Voland, R. T., and Wietıng, A. R., "*Calibration of the Langley 8-Foot High Temperature Tunnel for Hypersonic Air-breathing Propulsion Testing*", 19th AIAA Advanced Measurement and Ground Testing Technology Conference, New Orleans, LA, AIAA Paper 96-2197, 1996

[9] Garrard D., Rigney S., "*New Test Capability At AEDC2S Aerodynamic And Propulsion Test Unit (APTU)*", AEDC Group, USA

[10] Pescnke W.T., Barber T.J., Chıappetta L., Anderson T.J., Eckerle W.J., *"Hydrogen Fueled Scramjet Investıgatıon"*, United Technologies Research Center

[11] Yu G., Li, G., Zhang X., Chen L., Han XB., Sung C. J., *"Experimental Investigation On Flameholding Mechanism And Combustion Performance In Hydrogen-Fueled Supersonic Combustors"*, Laboratory of High Temperature Gas Dynamics, China

[12] Sullıns G.A., Waltrup P. J., Garrıtson G.R. *"The APL Alliances For High-Speed Aerothermal And Propulsion Testing"*, John Hopkins APL Technical Digest, Vol. 18, Number 2, 1997

[13] Dr. Satish Kumar & Team *"Scramjet Combustor Development"*, Head Hypersonic Propulsion Division & Dy. Project Director, HSTDV, DRDL, Hyderabad

[14] Krıshnan S, George Philmon, *"Solid Fuel Ramjet Combuster Design"*, Indian Institute of Technology Madras, India

[15] Andrews Ear, Torrence Marvin, Anderson Griffin, Northam Burton, Mackley Ernst, *"Langley Mach 4 Sramjet Test Facility"*, NASA Technical Memorandum 86277, 1985

[16] Andrews Earl, *"A Subsonic to Mach 5.5 Subscale Engine Test Facility"*, AIA A-87-2052, California, 1987

[17] Veraar Ronald, MAYER Alfons: *"The Role of the TNO Free Jet Test Facility in Solid Fuel Ramjet Projectile Development"*, TNO Defence, The Netherlands

[18] Ketchum Andrew, Emanuel Mark, Cramer John: *"Summary Of Rocketdyne Engine A5 Rocket Based Combined Cycle Testing"*, Boeing/Rocketdyne Propulsion and Power

[19] Turns S.R.: *"An Introduction to Combustion"*, McGraw-Hill Companies, Singapore, 2000

[20] Lefebvre A. H., Ballal D. R., *"Gas Turbine Combustion"*, CNC Press, 2010

[21] Law, C. K.: *"Combustion Physics"*, Cambridge University Press, New York, 2010

[22] Zucrow M. J., Hoffman J. D.: *"Gas Dynamics, Volume-1"*, John Wiley & Sons, Canada, 1976

[23] Glassman I.: *"Combustion "*, Academic Press Inc., Orlando, 1987

[24] Winterborne, D.E.: "*Advanced Thermodynamics for Engineers*", John Wley & Sons, New York, 1997

[25] Çengel Y. A., Boles M. A.: "*Mühendislik Yaklaşımıyla Termodinamik*", McGraw-Hill , Inc., İstanbul, 1996

[26] Cashdollar K. L., Zlochower I. A., Green G. M., Thomas R. A, Hertzberg M.: "*Flammability of Methane, Propane and Hydrogen Gases*", Journal of Loss Prevention in the Process Industries, Vol.13, pp. 327-340, 2000

[27] Mattingly J. D., Heiser W. H., Pratt D. T.: *"Aircraft Engine Design"*, AIAA, Virginia, 2002

[28] Walsh P. P., Fletcher P.: *"Gas Turbine Performance"*, Blackwell Science Ltd., Oxford 2004

[29] Headman O. P., Fletcher T. H., Graham S. G., Timothy G. W., Flores D. V., Haslam J. K.: "*Observations of Flame Behavior in a Laboratory Scale Premixed Natural Gas/Air Gas Turbine Combustor from PLIF Measurements of OH*", ASME Turbo Expo 2002, GT-2002-30052, Amsterdam, 2002

[30] Anderson J. D. : *"Fundamentals of Aerodynamics"*, New York, 2001

[31] Pope S. B., *"Turbulent Flows"*, Cambridge University Press, Cambridge, 2005

[32] Star CD Tutorials

[33] LINDE, Methane Material Safety Data Sheet

[34] http://www.cfd-online.com/Wiki/Turbulence_intensity, last updated on 20.06.2011

[35] Chen M., Hermann M., Peters N.:”Flamelet Modeling of Lifted Turbulent Methane/Air and Propane/Air Jet Diffusion Flames”, Proceedings of the Combustion Institute, Volume 28, 2000/pp. 167–174

APPENDICES

A. NASA SP 3001 TOTAL ENTHALPY DATABASE

T (K)	CH4	O2	N2	Ar	CO2	H2O
0	-20281.2	-2074.7	-2072.3	-1481.3	-96290.0	-60164.7
100	-19490.0	-1381.2	-1378.6	-984.4	-95594.5	-59378.5
200	-18694.1	-685.4	-683.0	-487.6	-94867.4	-58582.1
298.15	-17889.0	0.0	0.0	0.0	-94051.8	-57797.9
300	-17873.2	13.0	12.9	9.2	-94035.4	-57783.0
400	-16966.0	723.2	710.1	506.0	-93095.0	-56973.1
500	-15927.9	1454.3	1412.8	1002.8	-92066.6	-56143.4
600	-14746.8	2209.5	2125.8	1499.6	-90966.8	-55288.9
700	-13426.0	2987.5	2853.0	1996.5	-89808.3	-54407.3
800	-11973.7	3785.2	3596.2	2493.3	-88600.7	-53497.0
900	-10400.2	4599.2	4355.5	2990.1	-87352.1	-52557.0
1000	-8716.0	5426.9	5129.8	3486.9	-86069.3	-51586.5
1100	-6932.1	6265.8	5917.9	3983.7	-84757.7	-50585.6
1200	-5058.6	7114.3	6718.3	4480.5	-83421.9	-49554.6
1300	-3105.0	7971.0	7529.5	4977.3	-82065.6	-48494.8
1400	-1080.0	8835.0	8350.1	5474.2	-80691.9	-47407.4
1500	1008.6	9705.7	9179.0	5971.0	-79303.3	-46156.8
1600	3153.9	10582.6	10015.1	6467.8	-77901.8	-45156.8
1700	5350.0	11465.5	10857.6	6964.6	-76489.2	-43996.9
1800	7591.7	12354.2	11705.7	7461.4	-75066.8	-42816.1
1900	9874.3	13248.6	12558.8	7958.2	-73635.8	-41616.1
2000	12193.8	14148.6	13416.2	8455.0	-72197.3	-40398.2
2100	14546.9	15054.2	14277.6	8951.9	-70752.0	-39163.9
2200	16930.4	15965.3	15142.4	9448.7	-69300.6	-37914.2
2300	19341.8	16881.9	16010.5	9945.5	-67843.8	-36650.4
2400	21778.7	17803.9	16881.3	10442.3	-66382.0	-35373.5
2500	24239.1	18731.3	17754.8	10939.1	-64915.7	-34084.3
2600	26721.2	19664.0	18630.6	11435.9	-63445.3	-32783.7
2700	29223.5	20601.8	19508.6	11932.8	-61971.1	-31472.4
2800	31744.5	21544.7	20388.6	12429.6	-60493.4	-30151.1
2900	34283.2	22492.6	21270.4	12926.4	-59012.5	-28820.3
3000	36838.2	23445.4	22153.9	13423.2	-57528.4	-27480.6
3100	39408.8	24402.7	23038.9	13920.0	-56041.6	-26132.5
3200	41993.9	25364.7	23925.4	14416.8	-54552.0	-24776.5
3300	44592.9	26331.0	24813.3	14913.6	-53060.0	-23412.8
3400	47205.1	27301.5	25702.5	15410.5	-51565.5	-22041.9
3500	49829.7	28276.2	26592.8	15907.3	-50068.8	-20664.1